

**INVESTIGATION OF FLASH-FREE DIE CASTING BY OVERFLOW
DESIGN OPTIMIZATION**

Thesis

Presented in Partial Fulfillment of the Requirements for Master of Science
in the Graduate School of The Ohio State University

By

Sayak Roychowdhury B.E.E

Graduate Program in Industrial and Systems Engineering

The Ohio State University

2014

Master's Examination Committee:

Dr. Theodore T. Allen, Advisor

Dr. Jerald R. Brevick

Copyright by
Sayak Roychowdhury
2014

ABSTRACT

In die casting process, flash is a common problem caused by the impact pressure spike of the molten metal inside the die cavity. This can be attributed to the quick deceleration of the plunger when the cavity is full. Considerable waste of raw material, higher maintenance cost, low efficiency, high post processing cost are some of the adverse consequences of this phenomenon. The problem can be viewed from a design perspective, for instance, in SoftShot® technology the size of the overflows are designed to limit the pressure spike. In this research, this idea has been studied, using a hydraulic bench test and a mathematical optimization approach. The hydraulic bench test is set up to emulate the phenomenon of pressure spike caused by fluid flow. The pressure and the deceleration values are recorded for fluid flow through orifices of different size. In the second approach, a mathematical model for estimation of peak cavity pressure is optimized using Differential Evolution Algorithm and Nelder Mead Revised Simplex Search methods. Both of these methods indicate that the impact pressure can be minimized by implementing proper design of overflows.

To my parents Mr. Samar Kumar Roychowdhury and Mrs. Namita Roychowdhury

ACKNOWLEDGMENTS

I would like to convey my sincere gratitude to Dr. Jerald R. Brevick for his continuous guidance, encouragement and support in the course of this project. I would also like to thank Dr. Theodore T. Allen for all his support. Research Engineer William Tullos' help was indispensable during the setup and execution of the hydraulic bench-test. ISE Manufacturing Laboratory Supervisor Joshua Hassenzahl supported throughout. Last but not the least, I would like to thank Mr. Peter Ried of Ried and Associates for conceptualizing this project on behalf of NADCA, and for his guidance and valuable insights to ensure steady progress of this project.

VITA

June 2008B.E. Electrical Engineering,
Jadavpur University, India

July 2008 to June 2011Executive Engineer, Siemens, India

September 2011 to present..... Bonder fellow, Graduate Teaching
Assistant, Graduate Research Assistant,
Department of Integrated and Systems
Engineering, The Ohio State University,
USA

FIELD OF STUDY

Major Field: Industrial and Systems Engineering

TABLE OF CONTENTS

Abstract.....	ii
Acknowledgments	iv
Vita	v
Field of Study.....	v
table of contents.....	vi
list of tables	viii
LIST OF FIGURES	ix
Chapter 1 introduction	1
1.1 Flash-free Die Casting from a Design Perspective	3
Chapter 2 Literature review	5
Chapter 3 hydraulic bench test.....	8
3.1 Motivation.....	8
3.2 Bench Test Setup	9
3.3 Results.....	13
3.3.1 Phase 1	13
3.3.2 Phase 2	17
3.4 Bench Test Observations	22
Chapter 4 mathematical modeling of die casting process and optimization	23
4.1 Overview of SoftSHOT®	23
4.2 Issues with SoftShot® approach	26
4.3 Developing Mathematical Model in MATLAB®	27
4.4 Constraints for Overflow Design	31
4.5 Differential Evolution Algorithm	32
4.6 Differential Evaluation for optimization of Peak pressure	34
4.7 Nelder Mead Revised Simplex Search	36
4.8 Implementation of Nelder Mead RSS with SoftShot®.....	39
4.9 Comparison of two algorithms	41
Chapter 5 Discussions and Conclusion	42

Reference List.....	45
Appendix A: Plots from hydraulic bench test phase-2	48
Appendix B: specification sheets	62

LIST OF TABLES

Table 3.1 Observed and Calculated pressure spikes in Hydraulic Bench Test Phase-1	16
Table 3.2 Observed and Calculated pressure spikes in Hydraulic Bench Test Phase-2	18
Table 3.3 Added Runs in Phase-2.....	20
Table 4.1 Overflow dimensions for example 1 and 3 given in SoftShot® patent	24
Table 4.2 Optimal Solutions using DE	35
Table 4.3 Optimal solutions for peak pressure using NMRSS	40

LIST OF FIGURES

Figure 3.1 Schematic diagram of hydraulic bench-test	10
Figure 3.2 Accumulator and Solenoid Valves	11
Figure 3.3 Sensors	11
Figure 3.4 Bench test setup	12
Figure 3.5 Orifice setup	12
Figure 3.6 Orifices used in bench test	13
Figure 3.7 Recorded pressure and acceleration plot for orifice diameter 0.094 in.	15
Figure 3.8 Recorded pressure and acceleration plot for no orifice	15
Figure 3.9 Scatter plot of observed pressure spike w.r.t. orifice size	17
Figure 3.10 Plot of average pressure spike w.r.t. orifice size	17
Figure 3.11 Phase 2 Scatter plot of observed spike w.r.t. orifice size	19
Figure 3.12 Phase 2 plot of observed pressure spike w.r.t. orifice size with added runs ..	20
Figure 3.13 Phase 2 plot of average pressure spike w.r.t. orifice size	21
Figure 3.14 Observed and calculated pressure spike with respect to orifice area	22
Figure 4.1 Example 1 pressure and velocity profiles using SoftShot®	26
Figure 4.2 Example 3 pressure and velocity profiles using SoftShot®	26
Figure 4.3 Example 1 pressure and velocity profiles using MATLAB® prototype	30
Figure 4.4 Example 1 pressure and velocity profiles using MATLAB® prototype	31
Figure 4.5 Pressure and velocity profiles using 8 overflow gates with DE	35
Figure 4.6 Pressure and velocity profiles 8 overflow gates with NMRSS	40
Figure A. 1 Pressure and Acceleration for Phase-2 Shot 1	48
Figure A. 2 Pressure and Acceleration for Phase-2 Shot 2	48
Figure A. 3 Pressure and Acceleration for Phase-2 Shot 3	49
Figure A. 4 Pressure and Acceleration for Phase-2 Shot 4	49
Figure A. 5 Pressure and Acceleration for Phase-2 Shot 5	50
Figure A. 6 Pressure and Acceleration for Phase-2 Shot 6	50
Figure A. 7 Pressure and Acceleration for Phase-2 Shot 7	51
Figure A. 8 Pressure and Acceleration for Phase-2 Shot 8	51
Figure A. 9 Pressure and Acceleration for Phase-2 Shot 9	52
Figure A. 10 Pressure and Acceleration for Phase-2 Shot 10	52
Figure A. 11 Pressure and Acceleration for Phase-2 Shot 11	53
Figure A. 12 Pressure and Acceleration for Phase-2 Shot 12	53
Figure A. 13 Pressure and Acceleration for Phase-2 Shot 13	54
Figure A. 14 Pressure and Acceleration for Phase-2 Shot 14	54
Figure A. 15 Pressure and Acceleration for Phase-2 Shot 15	55
Figure A. 16 Pressure and Acceleration for Phase-2 Shot 16	55

Figure A. 17 Pressure and Acceleration for Phase-2 Shot 17.....	56
Figure A. 18 Pressure and Acceleration for Phase-2 Shot 18.....	56
Figure A. 19 Pressure and Acceleration for Phase-2 Shot 19.....	57
Figure A. 20 Pressure and Acceleration for Phase-2 Shot 20.....	57
Figure A. 21 Pressure and Acceleration for Phase-2 Shot 21.....	58
Figure A. 22 Pressure and Acceleration for Phase-2 Shot 22.....	58
Figure A. 23 Pressure and Acceleration for Phase-2 Shot 23.....	59
Figure A. 24 Pressure and Acceleration for Phase-2 Shot 24.....	59
Figure A. 25 Pressure and Acceleration for Phase-2 Shot 25.....	60
Figure A. 26 Pressure and Acceleration for Phase-2 Shot 26.....	60
Figure A. 27 Pressure and Acceleration for Phase-2 Shot 27.....	61
Figure A. 28 Pressure and Acceleration for Phase-2 Shot 28.....	61

Chapter 1

INTRODUCTION

Die casting is a metal casting process in which molten metal is injected into a mold cavity with high velocity, maintaining high pressure inside the cavity. In the cold chamber die casting process, the molten metal is ladled into the shot sleeve, which is then pushed forward into the cavity with the help of a plunger. The plunger is driven by hydraulic power. The hydraulic system typically consists of an accumulator, an inlet throttle valve and an outlet throttle valve. The valves are used to control the speed of the plunger.

In High Pressure Die Casting (HPDC), flash is a common phenomenon. According to NADCA Glossary about die casting, flash is “A thin web or fin of metal on a casting which occurs at die partings, vents and around movable cores. This excess is due to working and operating clearances in a die”. In a cycle of die casting process, metal pressure in the runner system is negligible until it reaches the main gate. Due to the restriction at the gate and high plunger velocity, pressure starts building up once the metal reaches the gate. When the cavity fills and metal starts flowing into the overflows, at that moment the pressure rises suddenly as the fast moving plunger comes to a halt. This pressure spike is often high enough to exceed the clamping force that holds die

halves together, followed by the occurrence of flash. Flash causes a number of problems in the process of HPDC. For instance it limits the speed of casting cycle (Milroy et al 1998) and results in wastage of material. Occurrence of flash requires the dies to be cleaned frequently, which in turn impedes the overall production process. Due to severe vibration at each shot, the tool life reduces significantly and frequent maintenance is required. Several techniques have been developed to prevent flashing, such as cryogenic trimming (freeze barreling) for castings without thin portions, component tumbling and short blast methods (Chives A.R.L, Zinc Die Casting). Machining processes are also used to remove flash (Milroy et al 1998). Since all of these require additional cost and secondary operations, producing flash-free castings would make the entire process much more efficient and cost effective.

The quality of the casting depends significantly on the pressure inside the cavity. The plunger velocity cannot be reduced under a certain point, and the intensification pressure has to be maintained in order to ensure the quality of the casting and satisfactory surface finish (Mickowski and Teufert 1993). After the completion of shot, the plunger applies pressure to the molten metal, known as 'intensification pressure' to minimize shrinkage porosity. The molten metal cools off and solidifies inside the cavity and eventually the die is open to eject the casting.

The cavity pressure depends on a number of factors. For instance, shot velocity, area of the gate, density of the molten metal, filling time, solidification of metal, volume of the cavity all affect the pressure inside the cavity after the shot is complete.

1.1 Flash-free Die Casting from a Design Perspective

In order to minimize the impact pressure spike, various techniques have been adopted and practiced, discussed in more detail in the next chapter. One idea is to modify the size of the overflows to contain the peak pressure at the time of the impact. This technique was named SoftShot®, which was proposed and patented by P. Olmsted. Overflows in die casting have been used traditionally for various reasons. For instance, overflows receive the molten metal entering first into the cavity, mixed with impurities and oxides. They act as a source of heat inside cavity, and help maintain steady temperature. Often they house the ejector pins, saving the part from having ejector pin marks. Air and gases are pushed to the overflows by the molten metal, and this ensures quality of casting. Hence the idea of designing overflows in order to reduce pressure spike is novel. To understand this method, a tour to the Port City Group, Muskegon, MI proved to be very helpful. Port City at first creates a MagmaSoft model to simulate the filling of the cavity to aid the overflow designs suggested by SoftShot®. Besides the reduction of impact pressure, adoption of this method has also resulted in downsizing shot cylinders and reducing injection velocity within the limits of required filling times. The procedure also facilitates cutting down the amount of die steel, greater tooling design options and increased dimensional control. Moreover, the vibration on the die casting machine is reduced significantly, tooling requires less maintenance and tool life has increased considerably.

Looking at the benefits of this approach, the idea of addressing the problem of flash from a design point of view seemed to be a potential research area in the field of die

casting. In this research, two different approaches were used to analyze and expand this idea of limiting the impact pressure by designing the overflows. The first approach was to conduct a hydraulic bench test in order to verify the idea if the size of the overflow could have an influence on the pressure spike at a small scale. Orifices of different size were used to perform a series of shots, and the peak pressure values are recorded. The bench test is described in Chapter 3, along with the results and observations.

The second approach was to optimize a mathematical model, used for estimation of the dynamic cavity and runner pressures and the plunger velocity. The model was built using the equations given in the SoftShot® patent document. Two different algorithms were used, viz. Differential Evolution Algorithm and Nelder-Mead Revised Simplex Search method in order to minimize the peak pressure. The results of the two algorithms are shown and compared in Chapter 4 of this document. The findings indicate that numerical optimization techniques can be used to design the overflows in order to minimize the peak impact pressure, thereby removing flash from die casting process.

Chapter 2

LITERATURE REVIEW

With the advancement of simulation technology, die designs are simulated to reduce the time and cost of actually building several dies in a trial and error fashion. Various techniques have been adapted to model fluid flow, heat transfer and solidification of molten metal. Minaie, Stelson and Voller (1991) used volume of fluid (VOF) method to model the fluid flow and an enthalpy technique on a fixed grid to model solidification. Cleary and Ha (1999, 2003, 2006) used a Lagrangian methodology known as Smoothed Particle Hydrodynamics (SPH) to model HPDC. Some researchers have implemented numerical analysis of gating systems in die casting. Sulaiman and Keen (1997) proposed a model to show variation in pressure with different branch angles for the overflows. Hu et al. (1999) used numerical simulation technique to design and optimize runner and gating systems for a magnesium telecommunication part. Esparza et al. (2005) used a gradient-search optimization technique to design an optimal gating system for gravity processes to produce aluminum parts. Palekar et al. (2008) proposed a coupled- motion numerical model for the plunger and liquid metal. Wu, Fuh and Lee (2007) presented a parametric system for designing the gating system for die casting.

Some research has been done to model the pressure inside the die cavity and to reduce flashing by controlling the impact pressure. Mickowski and Teufert (1993) put forward the technique of rapidly decelerating the plunger just before the impact in order to reduce the impact pressure using a closed loop control system with the hydraulic cylinder of the die casting machine. Xue et al (2011) developed a lumped parameter model for the cavity pressure spike. The SoftShot® process was explained by Branden, Olmsted and Kuhn (2002). Branden and Brown (2005) reported considerable process improvement after evaluating a tool design for an automotive transfer case using SoftShot®. The SoftShot® patent (Olmsted 2007) elaborates a mathematical model for the shot system in a die casting machine beginning at a hypothetical position when the cavity is full and molten metal is about to flow into the overflows. The model evaluates velocity of the shot system, pressure in the runner system, pressure in the cavity and position of the shot system (Branden and Brown 2005). The model is suitable for evaluating tooling and overflow designs. SoftShot® is also capable of calculating the volumes and cross sectional areas of orifices for a series of deceleration overflows, given the allowable maximum pressure. An iterative procedure was used to calculate the optimal dimensions of the overflows.

Attempts have been made to measure in-cavity pressure and temperature in die casting process. Hatamura et al. (1989) developed a pressure sensor and a heat flux/temperature sensor in order to measure these quantities inside die cavity and reported their findings on molten metal flow and solidification. Venkatasamy (1996) used Kistler pressure sensors to measure in-cavity pressure and thermocouple probes to measure temperature in view of development of a process control system. Tong et al. (2002) used

in-cavity pressure measurement for casting of a hand phone component to ensure product quality and also reported the relation between process variables and gate freezing time. Dargusch et al. (2005) measured molten metal pressure for casting of radio frequency filter box housing to investigate the relation among machine parameters, cavity pressure and casting quality. But there is no evidence of research based on in-cavity pressure measurement with dies of different designs of overflows, in order to observe the change in impact pressure. The hydraulic bench test described in chapter 3 is an attempt to emulate the pressure spike situation in the die casting machine to observe the change in impact pressure by varying the fluid flow through orifices of different size.

In chapter 4, the modeling technique of SoftShot® is used for calculating the peak pressure in the cavity for various overflow designs. Two mathematical optimization methods are implemented in order to minimize the peak pressure inside the cavity. The first method is a heuristic approach to minimize non-linear and non-differentiable functions, known as Differential Evolution algorithm (Storn, Price 1997). The second one is a variant of the direct search method called Nelder-Mead Simplex Search (Nelder and Mead 1965), known as Nelder Mead Revised Simplex Search (Humphrey and Wilson 2000) procedure. The outputs of these two procedures will be compared with the overflow dimensions suggested by SoftShot®.

Chapter 3

HYDRAULIC BENCH TEST

3.1 Motivation

A hydraulic bench was set up in order to analyze the nature of pressure spike during the flow of pressurized fluid through orifices. Till date, no research has been done on variation of in-cavity pressure spike with the change of design of overflows. Since die casting machines are complicated systems involving a large number of variables, a small scale emulation of the process involving fewer sources of variability seemed to be appropriate. The hydraulic bench test satisfied that requirement. The hydraulic fluid HF-28 was made to flow through orifices of different size. The fluid was pressurized by the hydraulic cylinder piston, moving at high velocity comparable to that of plunger velocity in high pressure die casting machines. Both molten metal and hydraulic fluid are incompressible, but there is no issue of solidification which might influence the magnitude of pressure spike. Hence the bench test can be looked upon as an instrument to effectively study the idea of reducing pressure spike by designing the overflows in the die cavity.

3.2 Bench Test Setup

The arrangement is shown in the schematic diagram figure 3.1. A hydraulic cylinder (9) (Parker 02.50 H2HL2S19 6.000) was pressurized at the head end with the help of an accumulator (4) (Tobul TBR-30-1-N) at 1000 psi. One of the ports at the rod end of the cylinder was connected to an arrangement of cross fittings (14). The cross fittings were analogous to the main cavity in the die casting setting. The free ends of the crosses were fitted with an orifice, equivalent to the overflow in a die. Through the other port, a pressure sensor (10) (Omega PX303 5KG5) was inserted to monitor the pressure of the hydraulic fluid. In order to create sufficient thrust at the piston end, two Hydac solenoid control valves (5 and 5a) were connected in between the head end ports of the cylinder and the accumulator. The accumulator was pressurized by a SPX (PA6M-1, 10000 psi) hydraulic foot pump (2). A vacuum pump (Welch 1400) (16) was connected to the cavity end cross fittings of the setup, in order to release the entrapped air in the system. A flip switch was used to actuate the solenoid valves 5 and 5a, upon triggering, the hydraulic pressure under accumulator would be applied to the head end of the piston. The piston would move, and the hydraulic fluid on the rod side of the piston would flow to the cross fittings, emulating the process of molten metal flow in die casting machine. The pressure sensor (10) would measure the pressure of the fluid, an accelerometer (Sparkfun SEN09332, type ADXL 193) (11) mounted on top of the piston would measure the acceleration and deceleration of the piston. Acceleration and pressure signals were acquired with the help of an NI 6009 USB data acquisition device (12). Pressure gauges (6) and (13) were used to monitor pressure at the accumulator and at the rod end of the

hydraulic cylinder respectively. At the end of the shot, the ball valve (7) was opened to let the hydraulic fluid go back to the reservoir. The specification sheets for the main components are provided in Appendix B. The bench test arrangement pictures are shown in figure 3.2-3.6.

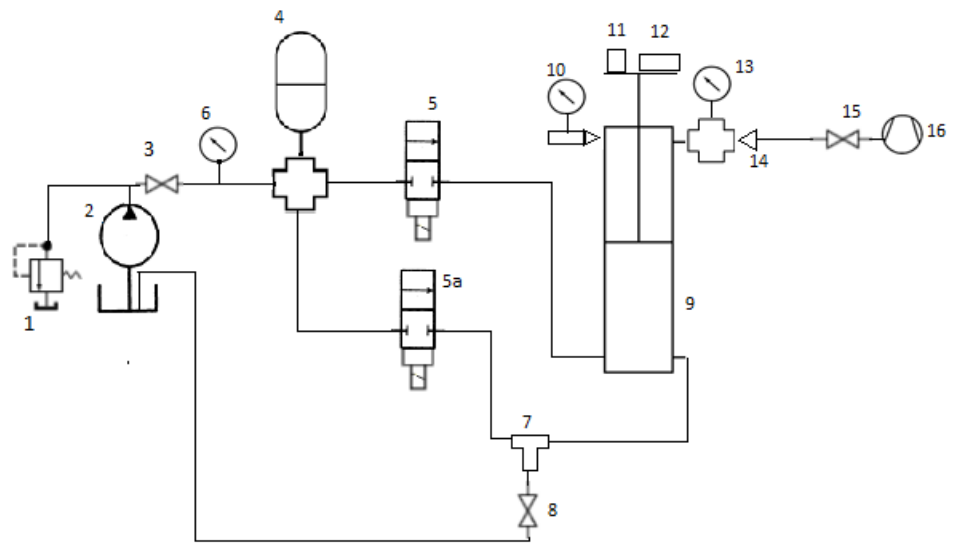


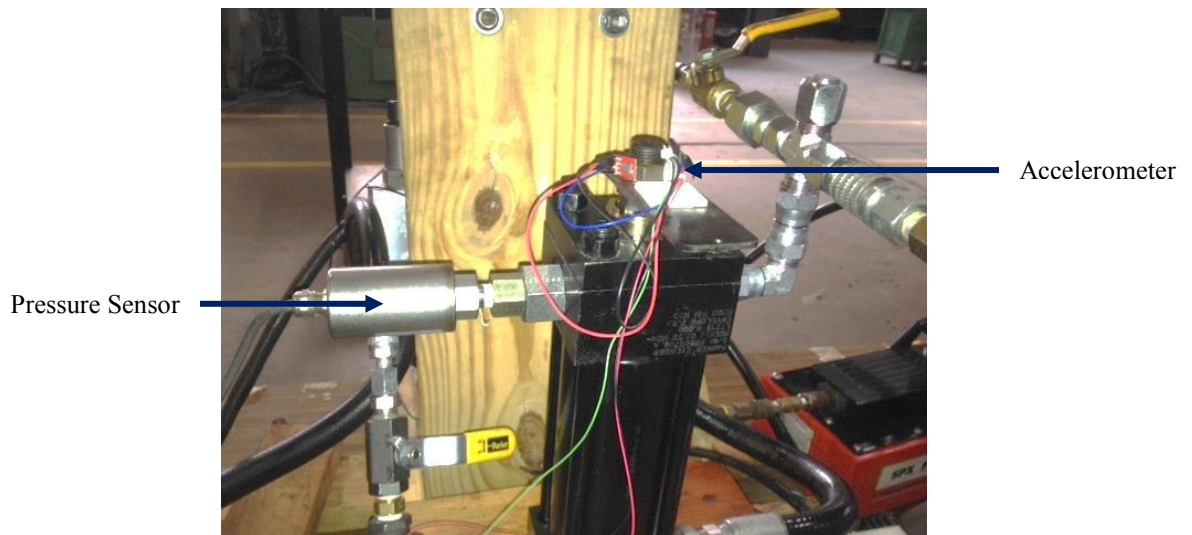
Figure 3.1 Schematic diagram of hydraulic bench-test



← Accumulator

← Solenoid Valve

Figure 3.2 Accumulator and solenoid valves



← Pressure Sensor

← Accelerometer

Figure 3.3 Sensors



Figure 3.4 Bench test setup



Figure 3.5 Orifice setup



Figure 3.6 Orifices used in bench test

3.3 Results

3.3.1 Phase 1

The bench test was conducted in 2 phases. In the first phase, orifices of six different diameters were used, ranging from 0.015 inch to 0.094 inch, and also the configuration without any orifice. Three replications were performed with each of the seven configurations. The run order was randomized in order to reduce the effect of uncontrollable factors. For all the runs, the accumulator precharge pressure was maintained at 550psi, and the accumulator was charged at 1000psi. The pressure and the acceleration data were collected at the rate of 20000 scans per second. A vacuum of -9 psi was created at the orifice side before each run. Before every shot, 6 cu.in (100ml) of hydraulic fluid was poured on the rod end of the cylinder. The cylinder was drained after completion of each shot, to minimize variability in mass of fluid. Table 3.1 shows the observed peak pressure, maximum deceleration and observed pressure spike for each shot. An estimate of pressure spike is also given in table 3.1, using the moving mass (approximately 5.54 lbs, with an upper limit of 9 lbs and lower limit of 5.35lbs, including the mass of hydraulic fluid at the rod end, head end and inside accumulator, mass of

piston). The observed pressure spikes were calculated from the difference between maximum pressure observed at each run and the steady state pressure attained at the end of the shot. The estimate for the pressure spike was calculated using the equation given below

$$Pressure\ Spike = \frac{(Maximum\ Deceleration) * (Moving\ Mass)}{Area\ of\ the\ bore\ of\ the\ cylinder - Area\ of\ piston\ rod}$$

Figures 3.7 and 3.8 are the plots of pressure and acceleration data collected during the bench test, for run 3 (using orifice of diameter 0.094 inches) and run 6 (with no orifice). The pressure spikes are quite conspicuous at the time of impact, showing an abrupt movement on the acceleration plot as well at the same time.

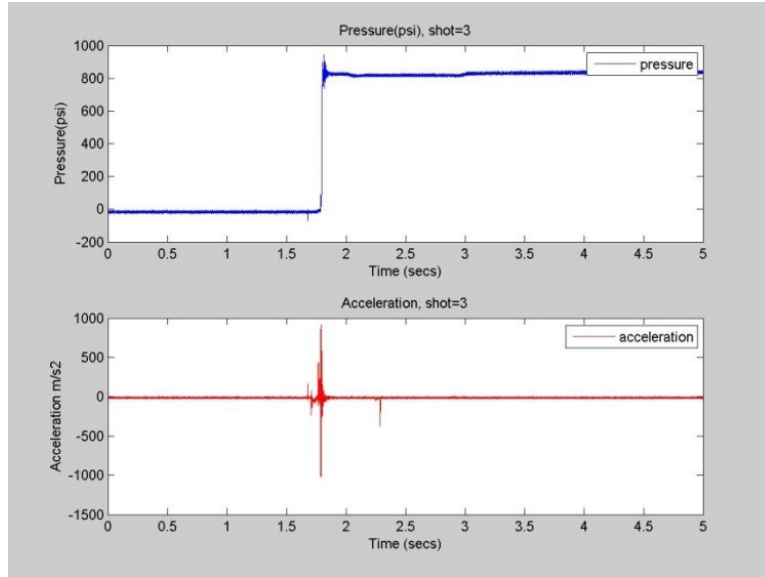


Figure 3.7 Recorded pressure and acceleration plot for orifice diameter 0.094 in.

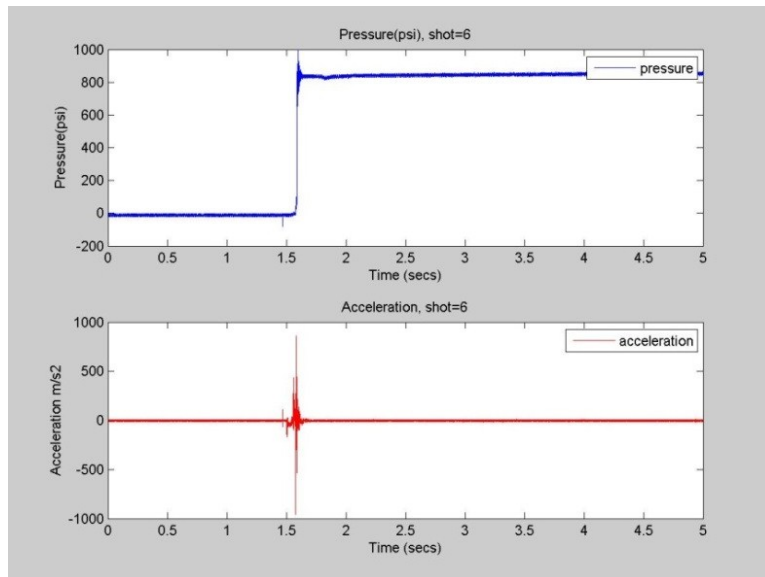


Figure 3.8 Recorded pressure and acceleration plot for no orifice

Run	Orifice Diameter (in)	Peak Pressure (psi)	Spike Observed (psi)	Calculated Spike (psi)	Max. Deceleration (inch/s²)
1	0.031	1013.02	187.144	151.7806	44603.85
2	0.062	1015.57	146.83	133.3621	39423.94
3	0.094	944.06	117.72	136.3168	40286.93
4	0.047	992.58	168.31	109.8388	32640.49
5	0.031	1007.91	179.45	167.4574	48958.17
6	0	997.69	164.07	128.4002	37611.74
7	0.062	987.48	156.33	131.9777	38721.58
8	0.078	961.94	131.569	160.0719	46786.52
9	0.062	936.64	129.72	149.8005	43826.68
10	0.015	982.37	159.21	189.1543	55247.92
11	0	967.04	146.52	188.9696	55247.92
12	0.047	928.73	125.98	201.3789	58947.91
13	0.047	954.27	114.74	165.852	48443.6
14	0	995.14	171.22	101.879	29748.37
15	0.031	972.15	157.1	172.2966	50320.37
16	0.015	969.6	144.39	225.2271	65797.11
17	0.015	946.61	134.63	225.5951	65886.88
18	0.078	887.87	76.7	179.3586	52395.56
19	0.094	938.95	129.39	182.5856	53334.15
20	0.078	880.21	65.38	177.9298	51977.46
21	0.094	936.4	121.1	119.6344	34957.8

Table 3.1 Observed and Calculated pressure spikes in hydraulic bench test phase-1

The scatter plot of the observed pressure spikes with respect to the orifice size is given in figure 3.9. The average values of observed pressure spike for each orifice size are plotted in figure 3.10. Apparently, there is a decreasing trend until the minimum spike occurs at the orifice of diameter 0.078 inch, after that the pressure spike increases. To have more insight on the variation of spike with the size of the orifices, and to observe more of the trend, phase 2 was planned, where orifices of larger diameter were used.

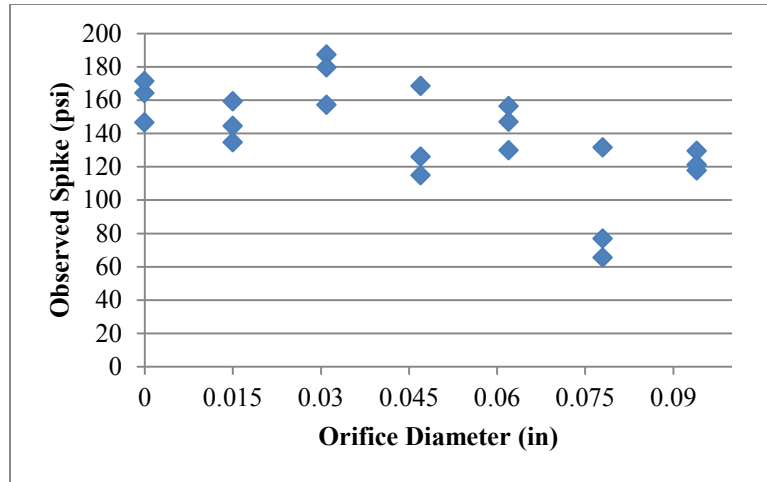


Figure 3.9 Scatter plot of observed pressure spike w.r.t. orifice size

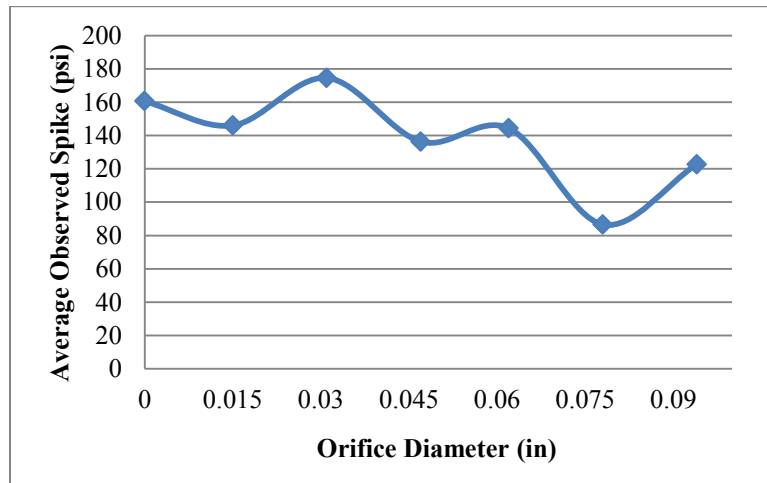


Figure 3.10 Plot of average pressure spike w.r.t. orifice size

3.3.2 Phase 2

In phase 2, orifices of 7 different diameters were used, together with the configuration without orifice. The orifice diameters ranged from 0.015 inch to 0.2 inch, as shown in Table 3.2. 4 orifices had diameter (0.11 inch, 0.14 inch, 0.17 inch and 0.2 inch) larger than the maximum diameter used in phase 1. Each configuration was

replicated 3 times, resulting in 24 runs altogether, keeping all the other conditions same as that of phase 1.

Run	Orifice Diameter (in)	Peak Pressure (psi)	Spike Observed (psi)	Calculated Spike (psi)	Acceleration (inch/s²)
1	0.2	992.58	169.25	164.85	48026.42
2	0.14	1069.21	253.21	201.59	58728.68
3	0.078	936.4	120.77	192.72	56145.5
4	0.047	892.98	102.84	161.69	47104.76
5	0.14	972.15	170.37	177.54	51721.73
6	0.11	949.17	147.28	204.82	59669.59
7	0.17	961.94	160.16	183.12	53347.51
8	0	931.29	120.56	167.11	48683.02
9	0.047	910.86	117.34	137.36	40016.13
10	0.11	951.72	142	188.70	54973.68
11	0.14	1025.79	211.63	194.71	56724.73
12	0.015	944.06	131.69	130.99	38161.41
13	0.2	1000.25	179.22	177.23	51631.02
14	0.015	946.61	130.2	140.69	40986.88
15	0	954.27	144.19	154.59	45036.01
16	0.17	1135.61	314.03	187.95	54756.52
17	0.2	987.48	154.1	154.77	45089.03
18	0.015	954.27	125.47	164.05	47792.77
19	0.047	928.73	124.88	179.53	52300.96
20	0	967.04	157.89	155.57	45320.72
21	0.078	903.49	98.7	150.71	43905.04
22	0.078	913.41	93.14	192.24	56003.73
23	0.17	974.71	157.46	167.26	48726.61
24	0.11	961.94	138.24	161.24	46973.2

Table 3.2 Observed and calculated pressure spikes in hydraulic bench test phase-2

The scatter plot of observed pressure spike with respect to orifice diameter is shown in figure 3.11.

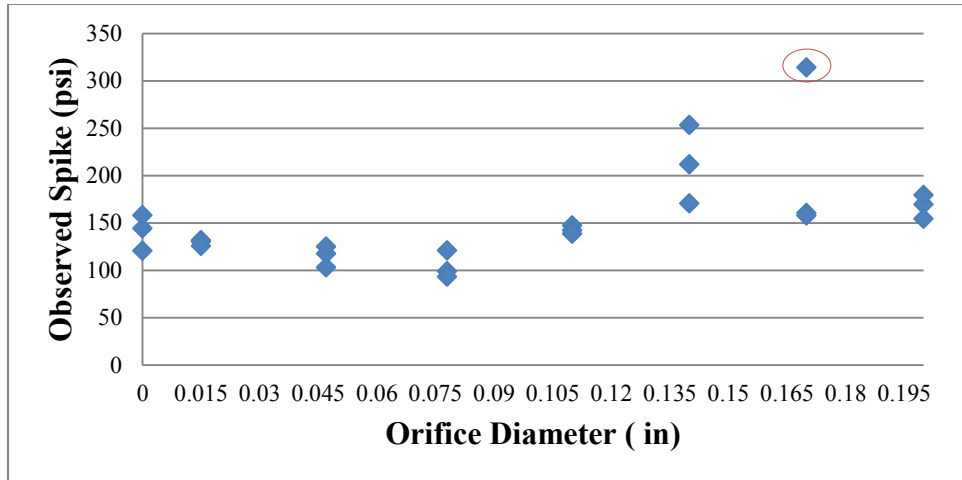


Figure 3.11 Phase 2 scatter plot of observed spike w.r.t. orifice size

The scatter plot in figure 3.11 supports the observation in phase 1, that the minimum spike occurred for orifice with diameter 0.078 inch, and then the spike increased for larger orifices. However, the deviations in observed spikes at orifices 0.14 inch and 0.17 inch were much greater than the rest. In fact, the point circled with red is possibly an outlier at 0.17 inch. Due to the higher uncertainty at these two points, 2 more replications with each of these 2 orifices were conducted, and runs 25-28 are shown in Table 3.3. Figure 3.12 shows the new scatter plot, and figure 3.13 shows the plot with average spike at each orifice. The outlier at orifice with diameter 0.17 inch was omitted in the calculation of average pressure spike for the plot in figure 3.13.

Run	Orifice Diameter (in)	Peak Pressure (psi)	Spike Observed (psi)	Calculated Spike (psi)	Acceleration (inch/s ²)
1	0.14	1064.1	247.54	148.28	43197.00
2	0.17	995.14	169.97	243.58	70960.89
3	0.14	1051.33	227.96	99.48	28981.26
4	0.17	984.92	170.67	129.40	37699.2

Table 3.3 Added runs in phase-2

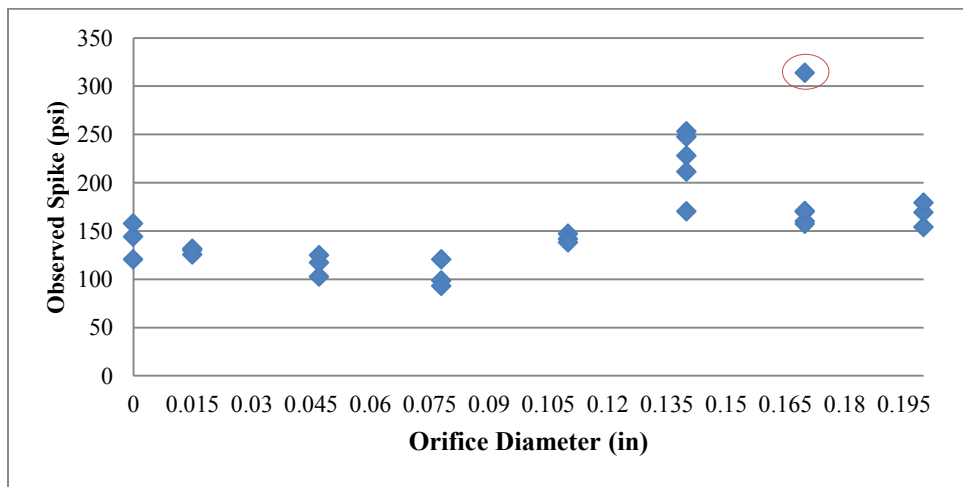


Figure 3.12 Phase 2 plot of observed pressure spike w.r.t. orifice size with added runs

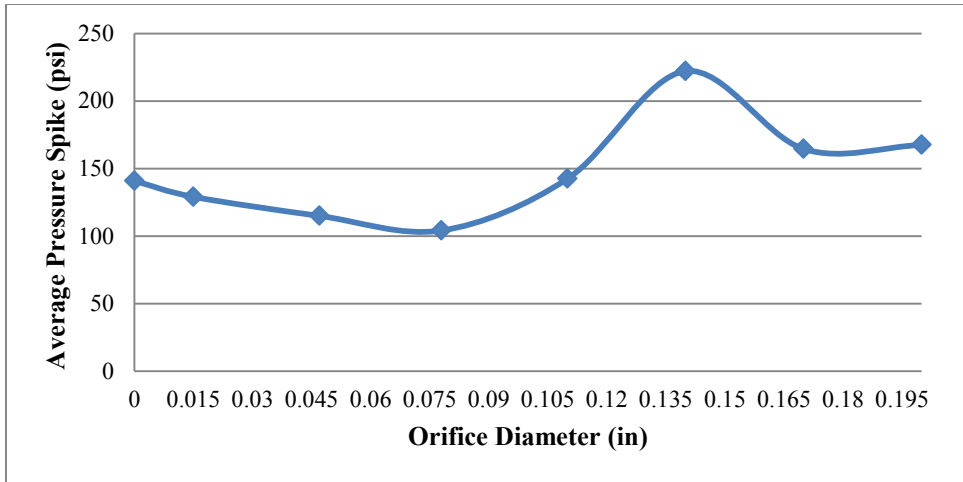


Figure 3.13 Phase 2 plot of average pressure spike w.r.t. orifice size

Figure 3.13 clearly shows, that the minimum pressure spike occurred with the orifice having diameter of 0.078 inch. Figure 3.14 shows the plot of observed values and calculated values for pressure spike for phase 2. The estimated values were much closer to the observed values for no orifice configuration, but were different for the other cases, since the orifice size has not been taken into consideration for the estimates.

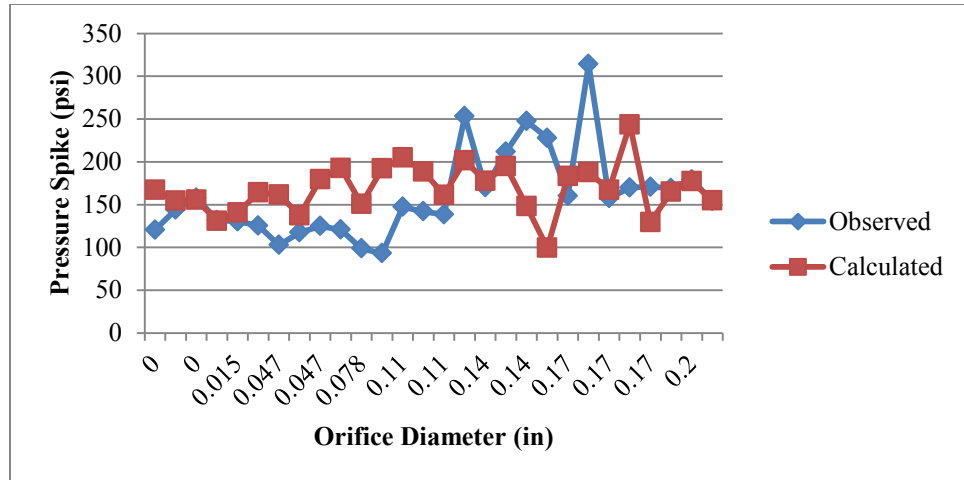


Figure 3.14 Observed and calculated pressure spike with respect to orifice area

3.4 Bench Test Observations

From phase 1 and phase 2 of the bench test, evidently, the orifice size considerably influenced the impact pressure spike. In the above tests, the pressure spike was minimum for the orifice with diameter 0.078 inch and increased for larger orifices. This finding suggests that the pressure spike inside the cavity of the die casting machine can be minimized by appropriately designing the overflows. In the next chapter, a mathematical model is furnished and two different optimization algorithms are used in order to achieve the optimal design of overflows with the objective of minimizing the pressure spike.

Chapter 4

MATHEMATICAL MODELING OF DIE CASTING

PROCESS AND OPTIMIZATION

4.1 Overview of SoftSHOT®

The SoftSHOT technology is an innovative idea which suggests that by designing the overflows, it is possible to control the deceleration of the plunger and thereby reducing flash significantly in the process of die casting (Branden and Brown 2005). The mathematical model associated with this method can calculate the cross-sectional area and the volume of a series of overflows which would contribute to absorb the kinetic energy imparted by the plunger. (Branden and Brown 2005) compared the design of these overflows with inefficient valves which cause high pressure drops at a given flowrate.

To demonstrate the effectiveness of this method, an example was given in the SoftSHOT® patent document. A ‘prior art’ design for overflows was considered in example 1, and the pressure inside the cavity, runner pressure, velocity and position of the plunger were calculated using the model. The overflow dimensions are given under ‘Example 1’ in Table 4.1. The machine parameters and initial conditions are given below:

Weight of the piston, plunger and tip (W) = 367 lbs

Plunger velocity at impact (V_0) = 130 in/sec

Diameter of piston (D_p) = 7.00 in

Diameter of piston rod (D_r) = 4.00 in

Diameter of the plunger tip (D_{tip}) = 4.50 in

Pressure of the accumulator (P_{acc}) = 980 psi

Pressure of the cold chamber at impact (P_c) = 709 psi

Weight of the trimmed casting (W_{cav}) = 1.15 lbs

Number of cavities in the mold (N_{cav}) = 2

Weight of the runner system (W_{run}) = 3.26 lbs

The value of mold expansion to molten metal compression (R_{ac}) = 2.0

($R_{ac}=1$ is used in MATLAB® model)

Casting metal = Magnesium

The overflow areas and volumes for examples 1 and 3 are given in table 4.1.

Example 1 (prior art)			Example 3 (SoftSHOT® recommended)	
Overflows	Area (sq. in)	Volume(cu.in)	Area (sq. in)	Volume(cu.in)
1	1.136	0.050	0.220	0.055
2	1.136	0.060	0.348	0.042
3	0.947	0.050	0.441	0.034
4	1.136	0.050	0.519	0.029
5	1.136	0.050	0.598	0.026
6	1.136	0.061	0.477	0.017
7	-	-	0.393	0.012

Table 4.1 Overflow dimensions for example 1 and 3 given in SoftShot® patent

Figure 4.1 shows the pressure and velocity profiles for example 1. The lines A5 and B5 represent cavity pressure and runner pressure respectively, as percentages of their corresponding maximum values. C5 represents the plunger velocity and D5 shows the distance travelled by the plunger. The peak pressure obtained is 13763 psi, which is considerably higher than the desired P_{\max} value, and hence the clamping force. Moreover, the negative velocity suggests that the plunger would bounce back and forth before coming to a stop. This may have adverse consequences on machine life and tooling. All of these indicate the shortcomings of the design and suggest against implementation of such a design.

To mitigate the excessive impact pressure spike, SoftShot® determined through an iterative process the volumes and areas of the overflows, which would limit the peak pressure to 3498 psi, within the specified P_{\max} value. The dimensions are shown under 'Example 3' of table 4.1. The pressure and velocity profiles are shown in figure 4.2. A7 and B7 represent the cavity and runner pressure values respectively, and C7 represent the plunger velocity. It is interesting to note that the velocity gets attenuated steadily and never goes negative, suggesting less severe vibration in the die casting machine, thereby lowering maintenance and longer tool life.

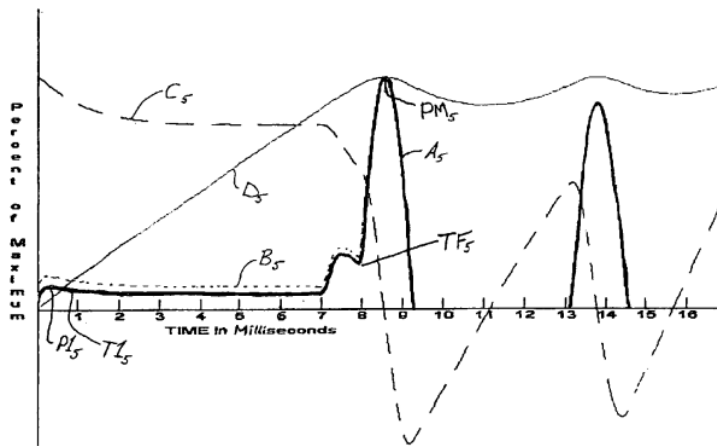


Figure 4.1 Example 1 pressure and velocity profiles using SoftShot®

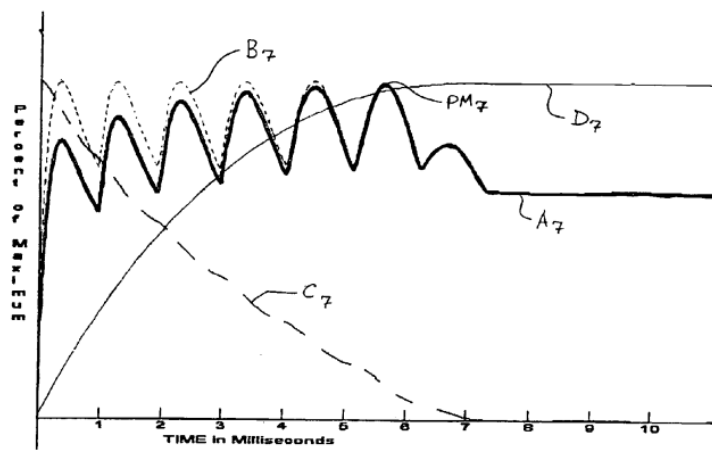


Figure 4.2 Example 3 pressure and velocity profiles using SoftShot®

4.2 Issues with SoftShot® approach

In the SoftShot® method, the user cannot specify a preferred number of overflows, or suggest a reasonable upper bound and lower bound on the size of the overflows. The dimensions solicited by this method may not be feasible to implement in

cases where number of overflows is too many to accommodate in the design. If the recommended dimensions are too small, then machining these overflows may seem to be physically impossible. Hence a method which will enable the users to apply this novel idea, with the additional capability of specifying the number of overflows and mentioning reasonable limits on dimensions appeared to be a natural extension in this field of research.

4.3 Developing Mathematical Model in MATLAB®

In the SoftShot® patent (Olmsted 2007), the equations required to estimate the dynamic pressure inside the cavity and runner and the velocity of the plunger are given. These equations are stated below.

At time $T=0$, the plunger is travelling at fast shot speed and cavity pressure is zero with all the overflow chambers being empty.

The net force applied by the piston at time T is given by

$$F_{pist} = (A_{pist} * P_{acc}) * \left(1 - \left(\frac{V}{V_0}\right)^2\right) + P_{mo} * A_{tip} * \left(\frac{V}{V_0}\right)^2 \quad (1)$$

Where V is the plunger velocity at time T , P_{mo} is the initial runner pressure, A_{pist} is the cross-sectional area of the piston and A_{tip} is the cross-sectional area of the plunger tip. Based on the value of the force imparted by the piston, the incremental velocity of the piston is given by,

$$dV = g * (F_{pist} - P_{run} * A_{tip}) * dT/W \quad (2)$$

dT is the time step in seconds (0.0005 milliseconds), g is the acceleration due to gravity (386 inch per second) .

The initial flow rate through main gate is $Q_0 = V_0 * A_{tip}$ (cubic inch per second).

At any instant T, the flow rate is Q, calculated in the following way,

$$\begin{aligned} Q &= Q_0 * \sqrt{(P_{run} - P_{cav})/P_{mo}} && \text{when } P_{run} \geq P_{cav} \\ Q &= -Q_0 * \sqrt{(P_{cav} - P_{run})/P_{mo}} && \text{when } P_{run} < P_{cav} \end{aligned} \quad (3)$$

Where P_{run} is the pressure in the runner system and P_{cav} is the pressure in cavity.

The flow rate through overflow gate is given by

$$\begin{aligned} QOV(i) &= F_{coeff} * Orf(i) * \sqrt{2 * g * P_{cav}/Denc} \quad \text{when } Vol(i) > Fill(i) \\ QOV(i) &= 0 \quad \text{when } Vol(i) \leq Fill(i) \end{aligned} \quad (4)$$

Orf(i) is the cross-sectional area of i^{th} overflow gate, Denc is the density of the molten metal and F_{coeff} is the flow coefficient, with the value 0.78. Vol(i) is the volume and Fill(i) is the volume of molten metal accumulated in the i^{th} overflow gate. The rate of filling for the i^{th} overflow is given by $QOV(i) * dT$. The incremental change in runner pressure is calculated as follows

$$dP_{run} = (V * A_{tip} - N_{cav} * Q) * RunRate * dT \quad (5)$$

The RunRate is the spring rate of the runner system, derived as

$$RunRate = E * \frac{Denc}{W_{run} * (1 + Rac)} \quad (5.1)$$

E is the modulus of elasticity of the molten metal.

The incremental change in cavity pressure in time dT is given by

$$dP_{cav} = Q - \sum_{i=1}^n QOV(i) * CavRate * dT \quad (6)$$

Where n is the number of overflows, and CavRate is calculated in the following way

$$CavRate = E * \frac{Denc}{W_{cav} * (1 + R_{ac})} \quad (6.1)$$

These equations are combined in a step by step integration process to develop the MATLAB® model. The motivation to build this model is to find an optimal arrangement of overflows to minimize peak cavity pressure using numerical optimization methods. The following changes and assumptions are made in the model:

1. Change in equation(4) in the above set of equations, to calculate the flow rate inside the overflow, the following relation is used in the MATLAB® model:

$$QOV(i) = F_{coef} * Orf(i) * \sqrt{2 * g * (P_{cav} - P_{Run}) / Denc}$$

when $Vol(i) > Fill(i)$

$$QOV(i) = 0 \quad \text{when } Vol(i) \leq Fill(i).$$

2. The value of R_{ac} (ratio of mold expansion to molten metal compression) is considered to be 1 instead of 2.
3. Modulus of Elasticity of Magnesium is considered to be $6.5 * 10^6$ psi, and the liquid density to be 0.0572 lb/in³. These values were not mentioned in the patent document.

To ensure the MATLAB® model behaves closely to the SoftSHOT® model, both example 1 and 3 are evaluated. Figure 4.3 and 4.4 are the plots generated from these two examples respectively. The peak pressure recorded was 13990.59 psi for example 1, whereas the SoftShot® generated value was 13763psi. The plot, though it looks similar to

that of the one generated by the SoftShot®, has a few noticeable differences. For instance, in the original SoftShot® plot in figure 4.1, the peak occurs at around 8.5 milliseconds, whereas, the same occurs at around 5 milliseconds in the plot generated by the MATLAB® prototype.

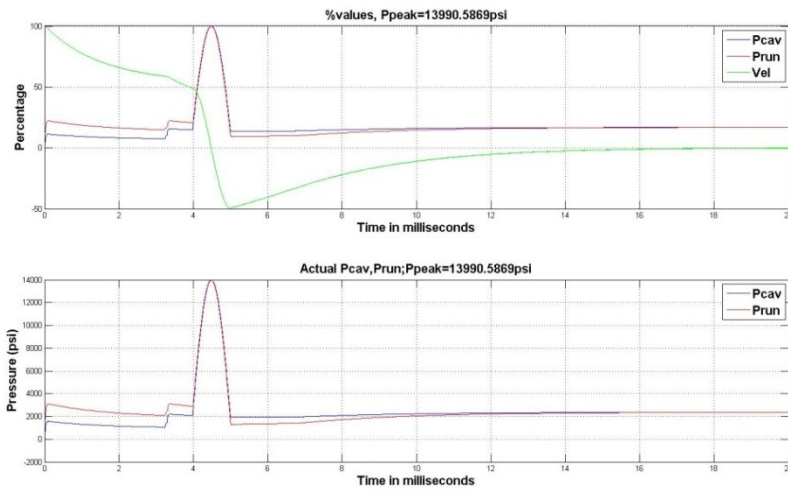


Figure 4.3 Example 1 pressure and velocity profiles using MATLAB® prototype

Figure 4.4 is the plot generated by the prototype using the example 3 overflow areas and volumes. The peak pressure recorded was 3537.51 psi, whereas the SoftShot® generated value was 3498psi. Comparing with figure 4.2, they appear to be reasonably close.

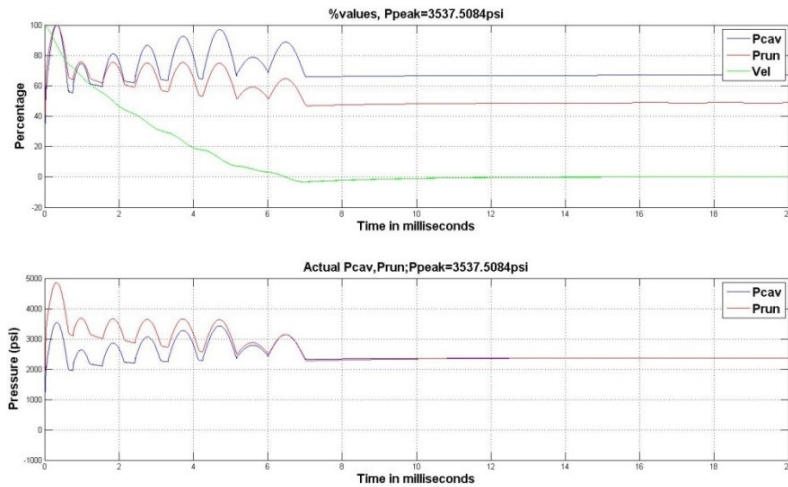


Figure 4.4 Example 1 pressure and velocity profiles using MATLAB® prototype

Based on the evidences above, the model is used for optimization using the Differential Evolution algorithm and Nelder Mead Revised Simplex. The algorithms and the outcomes are elaborated below.

4.4 Constraints for Overflow Design

For designing the overflows, several aspects have to be taken into consideration. The dimensions of the overflows typically depend on the shape and size of the cavity they are attached to, hence vary significantly from one die to another. However, a designer should adhere to some constraints while designing the overflows. For instance, since each overflow act as an extra heat source to the cavity (Thukkaram, 1972), having too many of them might add to the cycle time and require more cooling lines. Traditionally, trapezoidal or semi-circular cross-sections are used for overflows, and the thickness should be less than that of the main runner to ensure solidification before the

main gate. The overflows should be small enough for easy ejection, and multiple small overflows are preferred to one big overflow. The gate or feed of the overflows should be thin enough to facilitate easy trimming, but they should be strong enough to withstand ejection force as well. All of these have to be considered, and additionally there could be more constraints based on particular design requirements. Keeping in mind these criteria, the designer can decide upon the number of overflows and the upper and lower bounds on the size of the overflows.

4.5 Differential Evolution Algorithm

Differential Evolution (DE) is a heuristic approach to find global optimal solutions for non-linear functions (Storn, Price 1997). The advantages of DE include 1) it's capability of handling non-differentiable and multimodal functions, 2) it's parallelizability by using vector populations so that the stochastic perturbation of the population vectors can be done independently, 3) it has an efficient self-organizing scheme which is claimed to be superior than other evolution strategy algorithms and 4) good convergence properties. The DE algorithm consists of four steps, namely

Initialization: A population of size NP of D-dimensional vectors is created by randomly generated values with uniform distribution. This is done in order to cover the entire parameter space. If there is an initial solution available, the population can be created using deviations generated by normally distributed random values. The population vector in generation G is defined as

$x_{i,G}$ where $i = 1$ to NP

Mutation: New parameter vectors are generated by combining difference of two vectors with a certain weight (F) and adding it to a third vector. This process is called mutation. This is represented as follows

$$v_{i,G+1} = x_{r1,G} + F(x_{r2,G} - x_{r3,G}) \quad \text{where } i = 1 \text{ to } NP$$

$r1, r2$ and $r3 \in \{1, 2, \dots, NP\}$ are mutually different random numbers, which are also different from the index i and $F \in (0, 2)$.

Crossover: A trial vector u is formed

$$u_{i,G+1} = (u_{1i,G+1}, \dots, u_{Di,G+1})$$

Where

$$u_{ji,G+1} = \begin{cases} v_{ji,G+1} & \text{if } rand(j) \leq CR \text{ or } j = rndint(1 \dots D) \\ x_{ji,G} & \text{if } rand(j) > CR \text{ and } j \neq rndint(1 \dots D) \end{cases} \quad \text{where } j = 1 \dots D$$

CR is the crossover constant in the range $[0, 1]$, $rand(j)$ is a uniformly distributed random value $\in [0, 1]$, generated at the j^{th} time, and $rndint$ is a randomly chosen index between 1 to D .

Selection: The cost function using the trial vector $u_{i,G+1}$ is evaluated and if it renders a smaller value than the cost function using the target vector $x_{i,G}$, then $x_{i,G+1} = u_{i,G}$, otherwise the old value of $x_{i,G}$ is retained for the next generation.

These steps are repeated G times, and parameter vector in the G^{th} generation with the minimum cost function value is regarded as the solution.

4.6 Differential Evaluation for optimization of Peak pressure

DE algorithm is used to minimize the peak cavity pressure value, varying the cross-sectional areas and the volumes of the overflows. First 1 overflow gate is considered with the dimensions given in example 1, i.e. the prior art design as the initial values. Applying DE with 100 generations each of population size 200, the minimum peak pressure value found was 9354.2 psi. Then the number of overflows is incremented to 8, and the optimal peak pressure value came out to be 2258.3 psi. Table 4.2 shows the optimal solutions using number of overflows from 1 to 8, along with the time required to run the algorithm. The DE parameters used in this case were $F=1.5$ and $CR=0.7$. Figure 4.5 shows the plot of pressure and velocity profile, using 8 overflows. The initial values of 0.05sq.in. for diameter and 1.5 cu. in are used for orifices for each of this cases. The upper bound and the lower bound on the volumes are 2 cu. in and 0.2 cu.in. respectively.

Number of Overflows	Peak pressure (psi)	Volume (cu. in)	Orifice Area (sq. in)	Time Required (seconds)
1	9354.2	2	0.1500	395.65
2	6120.5	2.00, 2.00	0.0804, 0.1500	1345.63
3	4422.3	2.00, 2.00, 2.00	0.0661, 0.0402, 0.1500	1525.49
4	3586.1	2.00, 2.00, 2.00, 2.00	0.0358, 0.1412, 0.0642, 0.0100	1667.75
5	2903.1	2.00, 2.00, 2.00, 2.00, 2.00	0.1500, 0.0229, 0.0100, 0.0383, 0.0678	1836.62
6	2349.0	2.00, 2.00, 2.00, 2.00, 2.00, 2.00	0.0100, 0.0346, 0.1148, 0.0579, 0.0177, 0.0100	1987.41
7	2296.6	2.00, 2.00, 2.00, 2.00, 2.00, 2.00, 2.00	0.0100, 0.0162, 0.0100, 0.0531, 0.1124, 0.0100, 0.0300	2173.19
8	2258.3	2.00, 2.00, 2.00, 2.00, 2.00, 2.00, 2.00, 2.00	0.0100, 0.0100, 0.0153, 0.0100, 0.0100, 0.0435, 0.1165, 0.0278	2258.3

Table 4.2 Optimal solutions using DE

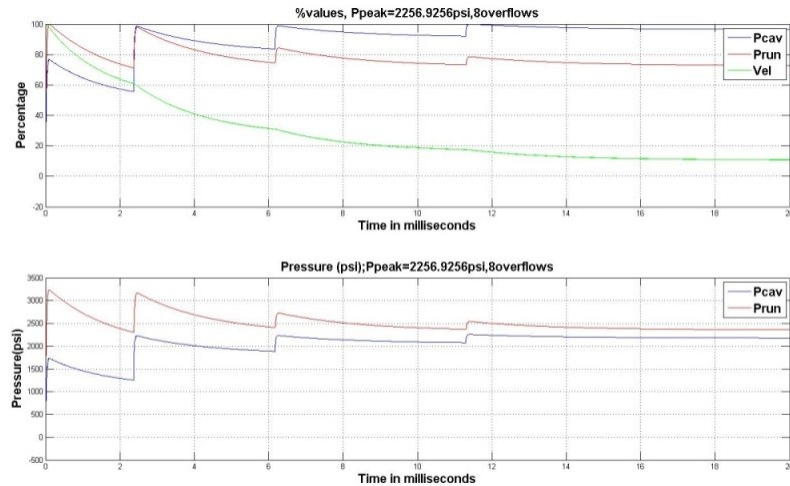


Figure 4.5 Pressure and velocity profiles using 8 overflow gates with DE

4.7 Nelder Mead Revised Simplex Search

The Nelder Mead is a direct search method for function minimization (Nelder, Mead 1960). This is a simplex procedure applied on a function of n variables, in which the function values are compared at $(n+1)$ vertices, among which the vertex with the highest value is replaced by another point. There are three operations, viz. reflection, expansion and contraction that are performed to modify the simplex and to arrive at the optimal solution. In the Revised Simplex Search (RSS) method (Humphrey and Wilson, 2000), the optimization is performed in three phases, and within each phase new simplexes are generated using reflection, expansion and contraction. RSS claims to adhere the desirable properties of the original Nelder Mead method, in addition, it is less affected by the choice of starting values, less prone to terminate at local optima and more robust in terms of handling noisy responses and computational efficiency.

The RSS procedure is described here in brief. Let $\hat{\theta}(x_i)$ be the function value at x_i where $i= 1,2,\dots,d+1$ and $x_i \in \mathcal{R}^d$. $\hat{\theta}_{max}$, $\hat{\theta}_{min}$ and $\hat{\theta}_{ntw}$ denote the maximum, minimum and next-to-worst values of the function at each stage q with x_{max} , x_{min} and x_{ntw} being the vertices respectively. Within phase ϕ , at each stage q (where $q= 1,2,\dots$) the centroid x_{cen} of all vertices are calculated, excluding the x_{max} .

$$x_{cen} = \frac{1}{d} \{ (\sum_{i=1}^{d+1} x_i) - x_{max} \} \quad (i)$$

In original RSS, the phase ϕ terminates when $\hat{\theta}$ meets the termination criterion. However, in order to ensure reasonable execution time, the execution of phase ϕ is ended if the number of stages q reaches 150 or the termination criterion is satisfied. The steps of the algorithm are described below:

- a) **Initialization:** The phase counter ϕ is set to 1 and the stage counter q is set to 0. The $d+1$ vertices are calculated as below

$$x_{i+1} = x_1 + v_1 e_i \text{ for } i = 1, 2 \dots d \quad (\text{ii})$$

$$\text{Where } v_1 = \begin{cases} \max\{\tau|x_{1,j}|:j = 1, 2 \dots d\} & \text{if } x_1 \neq 0_d \\ 1 & \text{otherwise} \end{cases}$$

x_1 is the initial vertex and e_i is a vector with the i^{th} element as 1 and rest being 0.

- b) **Reflection:** The reflected point x_{refl} is obtained in this step by reflecting x_{max} across x_{cen} or the centroid of the vertices excluding x_{max} .

$$x_{\text{refl}} = x_{\text{cen}} + \alpha(x_{\text{cen}} - x_{\text{max}}) \quad (\text{iii})$$

where α is the reflection coefficient and the value is taken to be 1, as considered in Nelder and Mead (1965). If $\hat{\theta}_{\text{min}} \leq \hat{\theta}_{\text{refl}} \leq \hat{\theta}_{\text{ntw}}$ then x_{max} is replaced by x_{refl} and the termination criterion (e) is checked. Otherwise step (c) is attempted.

- c) **Expansion:** If $\hat{\theta}_{\text{refl}} \leq \hat{\theta}_{\text{min}}$ then the search is extended towards the direction of $(x_{\text{refl}} - x_{\text{cen}})$ and the expansion point is obtained by

$$x_{\text{exp}} = x_{\text{cen}} + \gamma(x_{\text{refl}} - x_{\text{cen}}) \quad (\text{iv})$$

where the expansion coefficient $\gamma = 2.0$, as given in Nelder and Mead (1965). If $\hat{\theta}_{\text{exp}} < \hat{\theta}_{\text{min}}$ then the expansion is accepted and x_{max} is replaced by x_{exp} . Otherwise the expansion is rejected and x_{max} is replaced by x_{refl} . The termination condition (e) is checked followed by this. If $\hat{\theta}_{\text{refl}} > \hat{\theta}_{\text{min}}$, then the contraction step (d) is attempted.

- d) **Contraction:** If $\hat{\theta}_{\text{refl}} > \hat{\theta}_{\text{ntw}}$, then the size of the current simplex is reduced. If $\hat{\theta}_{\text{refl}} \leq \hat{\theta}_{\text{max}}$, then x_{refl} and $\hat{\theta}_{\text{refl}}$ replace x_{max} and $\hat{\theta}_{\text{max}}$ respectively. The contraction point is computed by

$$x_{\text{cont}} = x_{\text{cen}} + \beta(x_{\text{max}} - x_{\text{cen}}) \quad (\text{v})$$

where the contraction coefficient $\beta = 0.5$, as given in Nelder and Mead (1965). If $\hat{\theta}_{\text{cont}} \leq \hat{\theta}_{\text{max}}$, then x_{max} is replaced by x_{cont} . Otherwise

(if $\hat{\theta}_{cont} > \hat{\theta}_{max}$), the lengths of all the edges of the current simplex are reduced to produce a new simplex. The vertices are given by

$$x_i = x_{min} + \delta_\varphi(x_i - x_{min}) \text{ for } i= 1, \dots, d+1 \quad (\text{vi})$$

δ_φ is a shrinkage factor. The termination condition (e) is checked.

- e) **Termination criterion at each stage:** After each of the above steps, the following termination criterion is checked.

$$\max |x_i - x_{min}| \leq \begin{cases} \eta_1 |x_{min}|, & \text{if } |x_{min}| \neq 0 \\ \eta_2 & \end{cases} \text{ for } 1 \leq i \leq d + 1 \quad (\text{vii})$$

Where η_1 and η_2 are user specified tolerances. If the condition (vii) is not satisfied, the stage counter q is incremented by 1, and the steps are repeated from reflection again.

- f) **Final termination:** The termination point of current phase is recorded $x^*(\varphi) = x_{min}$ and the phase counter is incremented $\varphi = \varphi + 1$. When $\varphi > 3$, the final optimal solution is given by

$$x^* = \arg \min \{ \hat{\theta}(x^*(\varphi)) \text{ where } \varphi = 1, 2, 3 \}$$

If $\varphi \leq 3$ then the next phase is set up by setting the counter $q=0$. The initial values and the parameters v and δ_φ are updated in the following way

$$x_1 = x^*(\varphi - 1)$$

$$v_\varphi = 0.5v_{\varphi-1}$$

$$\delta_\varphi = \delta_{\varphi-1} + 0.2$$

4.8 Implementation of Nelder Mead RSS with SoftShot®

The NMRSS optimization procedure is implemented in order to minimize the peak pressure inside the cavity with the volumes and the cross sectional areas of the overflow gates as the decision variables. The optimization is done over 1 to 8 gates. The upper bound and the lower bound on the volumes are 2 cu. in and 0.2 cu.in respectively. For the cross-sectional areas, these values are 0.15 sq. in. and 0.01 sq.in. The initial value for volumes is 1.5 cu. in. and for areas is 0.05 sq. in. Table 4.3 shows the peak pressure values and the corresponding overflow gate dimensions when the modulus of elasticity E is considered to be 6.5×10^6 psi, and density of molten metal is 0.0572 lb/cu.in. The right-most column gives the time required by the Nelder Mead algorithm to find the optimal solution for each number of overflows.

Number of Overflows	Peak pressure (psi)	Volume (cu. in)	Orifice Area (sq. in)	Time Required (seconds)
1	7201.5	1.99	0.1305	13.94
2	4014	1.99, 1.88	0.0632, 0.1500	133.89
3	3115	1.28, 1.99, 1.99	0.1499, 0.0388, 0.0883	345.68
4	3193.6	2.00, 1.88, 0.7, 2.00	0.0374, 0.0182, 0.0910, 0.0745	564.08
5	2357.7	2.00, 1.88, 1.98, 2.00, 0.73	0.0385, 0.0720, 0.0178, 0.0878	913.85
6	2364.8	1.95, 1.66, 0.21, 1.25, 1.96, 1.97	0.0213, 0.1154, 0.1430, 0.0496, 0.0176, 0.0392	1178.4
7	2271.2	1.99, 1.84, 1.99, 1.61, 1.94, 1.68, 0.25	0.0174, 0.0162, 0.0166, 0.1066, 0.0277, 0.0496, 0.0950	1373.91
8	2188.9	1.03, 1.93, 0.70, 1.55, 1.96, 1.85, 2.00, 2.00	0.0134, 0.0169, 0.0921, 0.0652, 0.0162, 0.0354, 0.0173, 0.0158	1723.02

Table 4.3 Optimal solutions for peak pressure using NMRSS

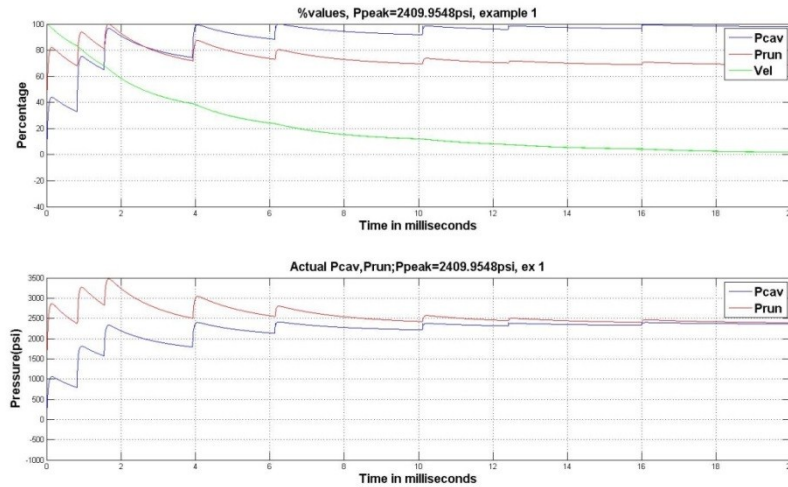


Figure 4.6 Pressure and velocity profiles 8 overflow gates with NMRSS

In the SoftShot® patent examples, the maximum pressure allowed was 3500 psi, and the best solution achieved was 3498 psi using the 7 overflows with sizes described example 3, compared to that, both DE and Nelder Mead had obtained peak pressure values of much smaller magnitude. With 8 overflows, the peak cavity pressure estimated was 2188.9 psi using Nelder Mead and 2258.3 psi using DE.

4.9 Comparison of two algorithms

From the results shown above, Nelder Mead provides marginally better solutions for almost all the cases, and also Nelder Mead takes less time. The time required by DE changes with the number of generations and the population size. The number of function evaluation for DE was 200000 for all the cases presented here. From the above approach, it is evident that a mathematical optimization technique can be used to determine the optimal design of overflows to minimize the peak pressure inside the cavity. Moreover, with this approach, the user has the choice to specify the number of overflows and also the upper and lower bounds on the size of the overflows. If the outcome for a particular number of overflows is not satisfactory, the user can vary the number and observe the solutions in order to make a final decision on the design of the cavity.

Chapter 5

DISCUSSIONS AND CONCLUSION

The goal of the present research is to approach the problem of flash from a design perspective, and study the idea of achieving flash-free die casting by designing the overflows. Two different approaches are described here to analyze the effect of changing overflow sizes in order to control the pressure spike at the end of the travel of the plunger. The first approach was to observe the pressure spike values obtained from a hydraulic bench test using orifices of different size. The second approach was optimization of a mathematical model, based on the equations provided in the SoftShot® patent using two different algorithms, viz, Differential Evolution and Nelder Mead Revised Simplex Search. The hydraulic bench test indicated that for a specific orifice size, the pressure spike attains the minimum. The modeling and optimization approach furnished the optimal design of overflows to minimize the pressure spike inside cavity for a particular die design and given machine parameters. Both of these approaches indicated that design of the overflows can have considerable effect on the impact pressure of the die casting process and proper design can ensure elimination of flash from the system.

Some measurement errors might have influenced the data collected from the bench test. The accelerometer used had a sensitivity of 8mv/g. The acceleration data collected by the accelerometer might include the effect of vibration of the entire bench as a result of the quick movement of the cylinder and coming to a sudden stop. Since the shots were replicated for each run and the setup was the same for all the shots, those effects should not be significant on the relative differences among the pressure spikes from shot to shot. The randomization of the run order also helped suppressing the effects of other factors such as difference in volumes of fluid discharged from the accumulator from shot to shot or loss of precharge pressure of the accumulator from influencing the outcome in general. If more replications were taken for each orifice size, the pressure spikes could be found to be converging towards particular values.

The performance of the DE algorithm could be changed by varying the parameters F and CR. Also, by increasing the number of generations and the population size might help towards reaching a better solution. But more often, the improvement is marginal compared to the rise in computational cost. Still it would be interesting to observe if the optimal solutions change significantly for a much higher number of generations and population size.

There are multiple research avenues that can be pursued from here onwards. The optimal solutions found using the algorithms can actually be implemented on a die similar to that described in the patent example. The pressure inside the cavity can be measured using a pressure sensor, and it will be interesting to see how much reduction in pressure spike can be achieved using the overflows suggested by the algorithms. It might be difficult to manufacture such overflows in the first place, since the sizes are not

standard for most of the time. Also, the model does not provide the location of the overflows, so that have to be determined separately. Using a simulation software to estimate where the molten metal will reach last might be one way to resolve this issue.

REFERENCE LIST

1. Branden J., Olmsted P., Kuhn C.W., Plunger Deceleration of a Die Casting Shot end – Applying Peter Olmsted SoftSHOTM Simulation Software, NADCA Congress, 2002
2. Branden J.T., Brown M., A Method for Developing Uniform Cavity Pressure, Extending Die Life by Integrating SoftSHOT Technology Onto Automotive Transfer Case Die, NADCA Transactions, 2005
3. Cleary P.W., Ha J., Three Dimensional Modeling on High Pressure Die Casting, 2nd International Conference in the Minerals and Process Industries, CSIRO, Melbourne, December 1998
4. Cleary P.W., Ha J., Prakash M., Nguyen T., SPH: A New Way of Modeling High Pressure Die Casting, 3rd International Conference in the Minerals and Process Industries, CSIRO, Melbourne, December 2003
5. Cleary P.W., Ha J., Prakash M., Nguyen T., 3D SPH Flow Predictions and Validation for High Pressure Die Casting of Automotive Components, Applied Mathematical Modeling (30), 2006
6. Dargusch M.S., Savage G., Wang G., Schauer N., Dinnis C.M., High Pressure Die Cast Aluminium Telecommunication Components, Transactions NADCA 2005
7. Esparza C.E., Guerrero-Mata M.P., Rios-Mercado R.Z. Optimal Design of Gating Systems by Gradient Search Methods, Computational Material Science, 36, 2006
8. Hatamura Y., Shirahige K., Mochigu Y., Takeda S., Direct Measurement of Metal Pressure and Die Surface Temperature, Transactions NADCA 1989, Paper No. G-T89-023
9. Humphrey D.G., Wilson J.R., A Revised Simplex Search Method for Stochastic Simulation Response Surface Optimization, INFORMS Journal on Computing, Vol12, No. 4, Fall 2000

10. Mickowski J.R., Teufert C.E., The Control of Impact Pressure in the High Pressure Die Casting Process, NADCA Transactions, 1993, pg 349-354
11. Milroy J., Hinduja S., Davey K., Modelling the pressure die casting process with the boundary element method: Die deformation model for flash prevention; Journal of Mechanical Engineering Science, 1998 212:197
12. Minaei B., Stelson K.A., Voller V.R., Analysis of Flow Pattern and the Solidification phenomenon in Die Casting Process, Journal of Engineering Materials and Technology, Transactions of the ASME, July 1991
13. Nelder J.A., Mead R. (1965) A simplex method for function minimization. Computer Journal 7 308-313
14. Olmsted, P. Method of Sizing Overflow Chambers, US Patent 7174947 B2, 2007
15. Palekar A., Starobin A., Reikher A., Die-casting end-of-fill and Drop Forge Viscometer Flow Transients Examined with a Coupled-motion Numerical Model, World Foundry Congress, 2008, pp 87-91
16. Shamshuddin S., Keen T.C., Flow Analysis Along the Runner and Gating System of a Casting Process, Journal of Materials Processing Technology, 63,1997
17. Storn R., Price K. (1997) , Differential Evolutions- A Simple and Efficient Heuristic for Global Optimization over Continuous Spaces; Journal of Global Optimization (11) 341-359
18. Thukkaram P., Factors Controlling Design of Runners, Gates, Overflows and Vents in Die Casting Dies, Transactions of the Seventh SDCE International Die Casting Congress, 1972
19. Tong K.K.S., Hu B.H., Niu X.P., Pinwill I., Cavity Pressure Measurements and Process Monitoring for Magnesium Die Casting of a Thin-wall Hand-phone Component to Improve Quality, Journal of Materials Processing Technology(127) 2002.
20. Venkatasamy V.K., Analysis of in-cavity Thermal and Pressure Characteristics in Aluminum Alloy Die Casting, Master of Science Thesis 1996, The Ohio State University
21. Wu S.H., Fuh J.Y.H., Lee K.S., Semi-automated Parametric Design of Gating Systems for Die-casting Die, Computers and Industrial Engineering,53,2007

22. Xue H., Kabiri-Bamoradian K., Miller R.A., Wang Y., Modeling Dynamic Pressure in High Pressure Die Casting Using Lumped Parameter Model, NADCA 2011
23. Zheng J., Wang Q., Zhao P., Wu C., Optimization of High Pressure Die Casting Parameters Using Artificial Neural Network, International Journal of Advanced Manufacturing Technology (2009)

APPENDIX A: PLOTS FROM HYDRAULIC BENCH TEST

PHASE-2

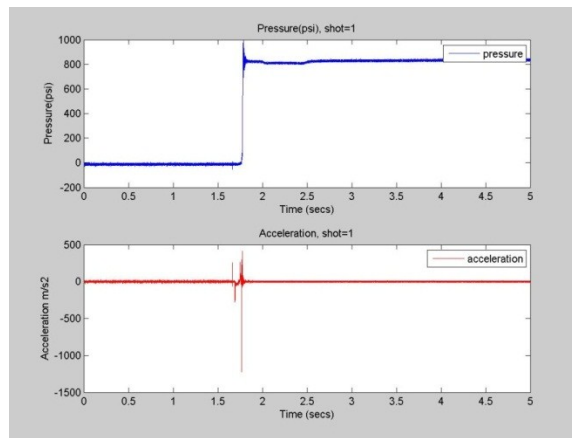


Figure A. 1 Pressure and Acceleration for Phase-2 Shot 1

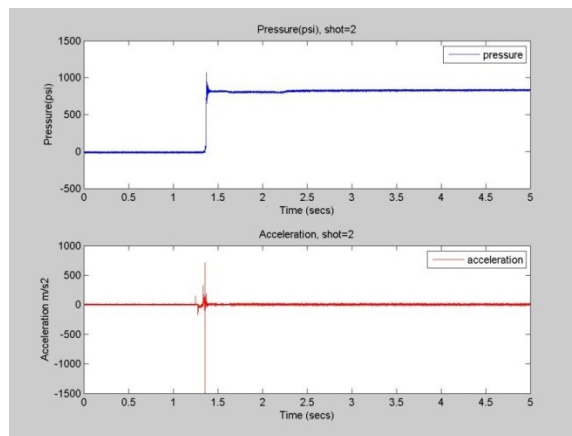


Figure A. 2 Pressure and Acceleration for Phase-2 Shot 2

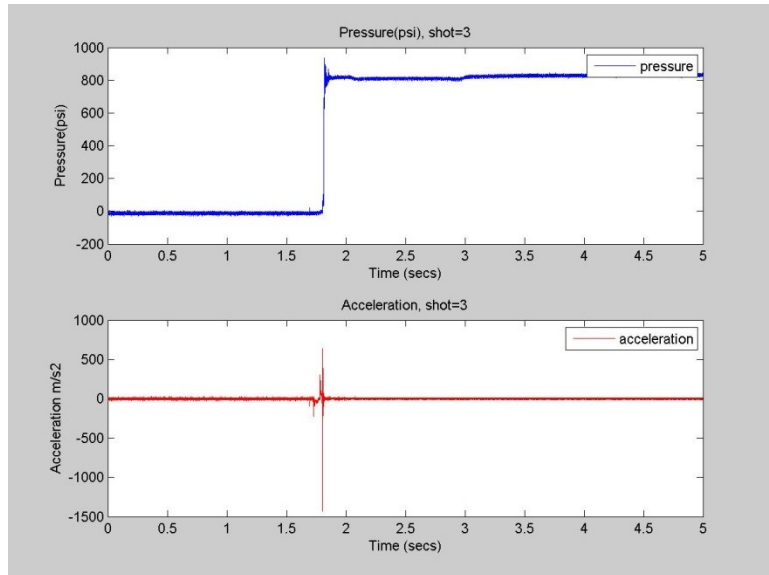


Figure A. 3 Pressure and Acceleration for Phase-2 Shot 3

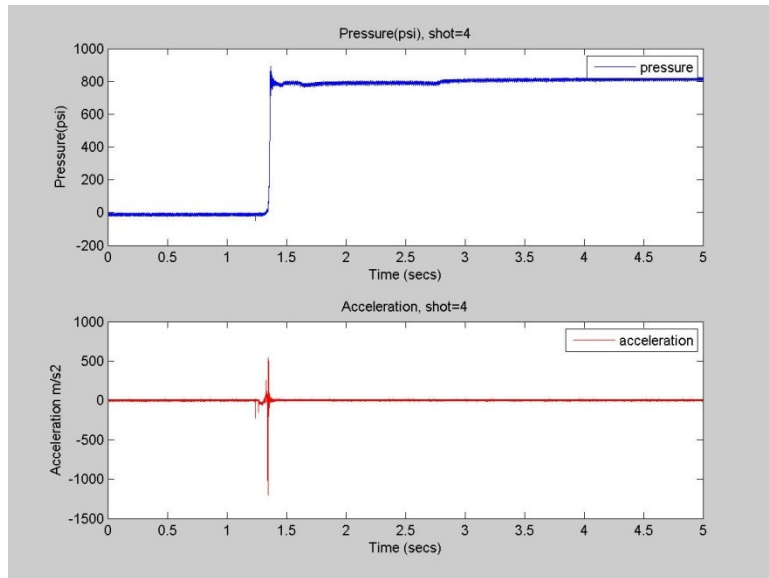


Figure A. 4 Pressure and Acceleration for Phase-2 Shot 4

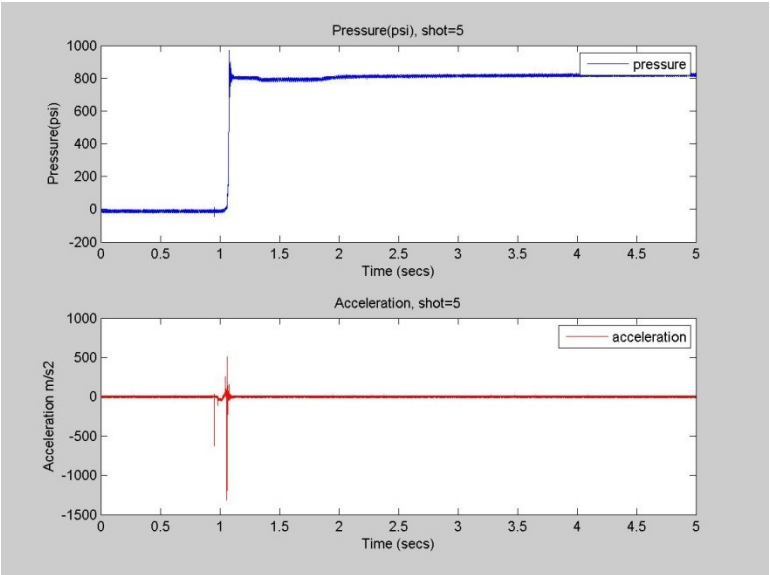


Figure A. 5 Pressure and Acceleration for Phase-2 Shot 5

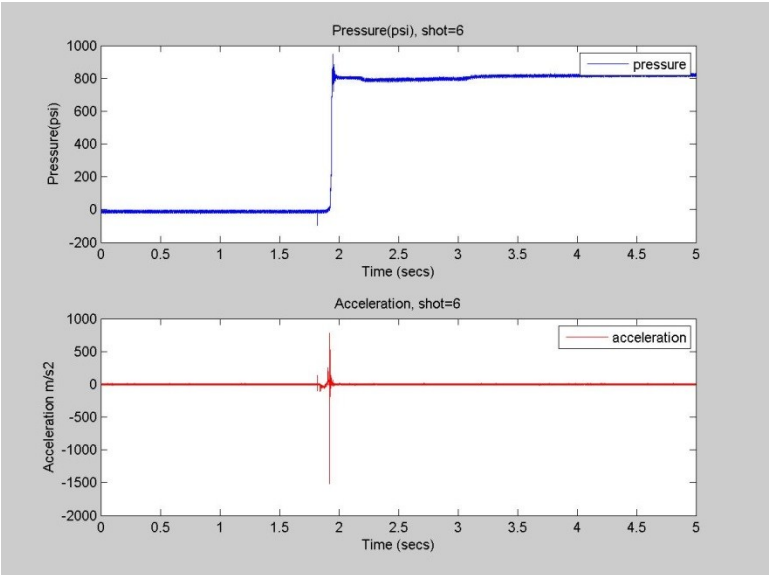


Figure A. 6 Pressure and Acceleration for Phase-2 Shot 6

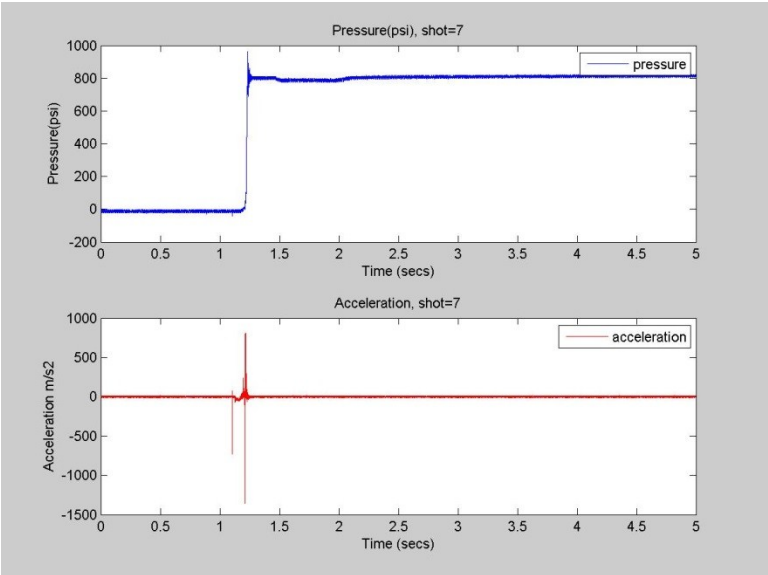


Figure A. 7 Pressure and Acceleration for Phase-2 Shot 7

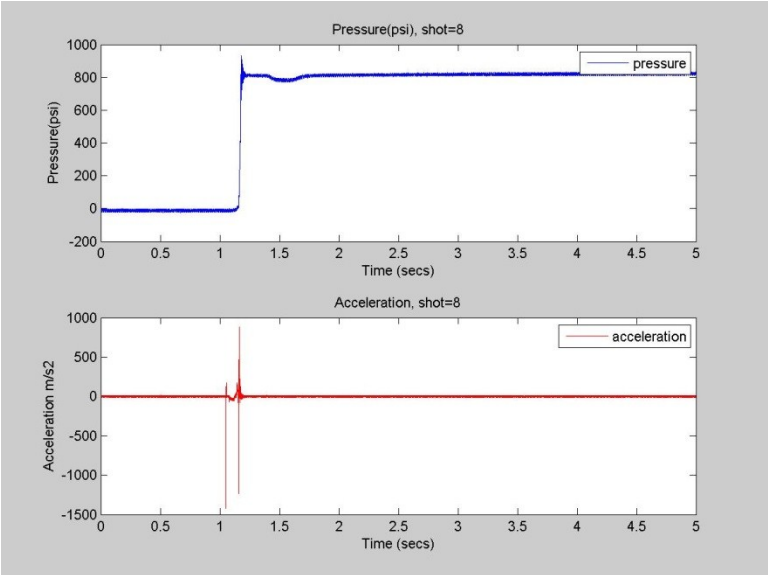


Figure A. 8 Pressure and Acceleration for Phase-2 Shot 8

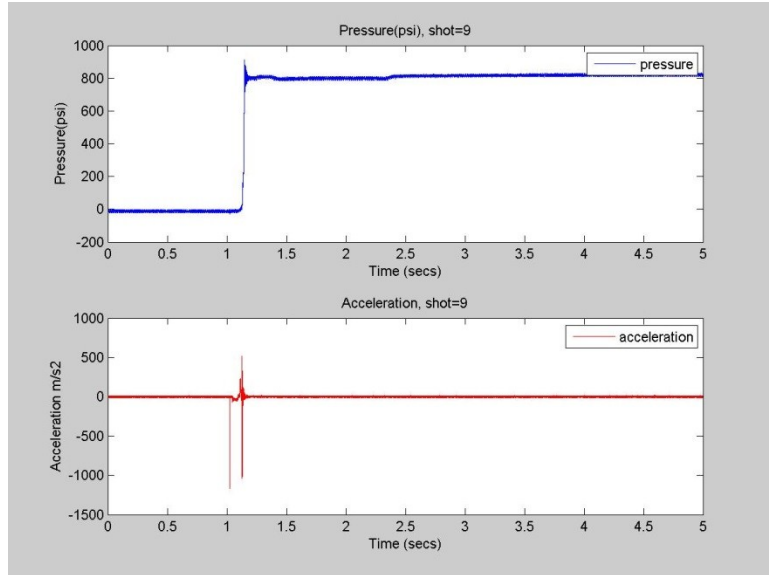


Figure A. 9 Pressure and Acceleration for Phase-2 Shot 9

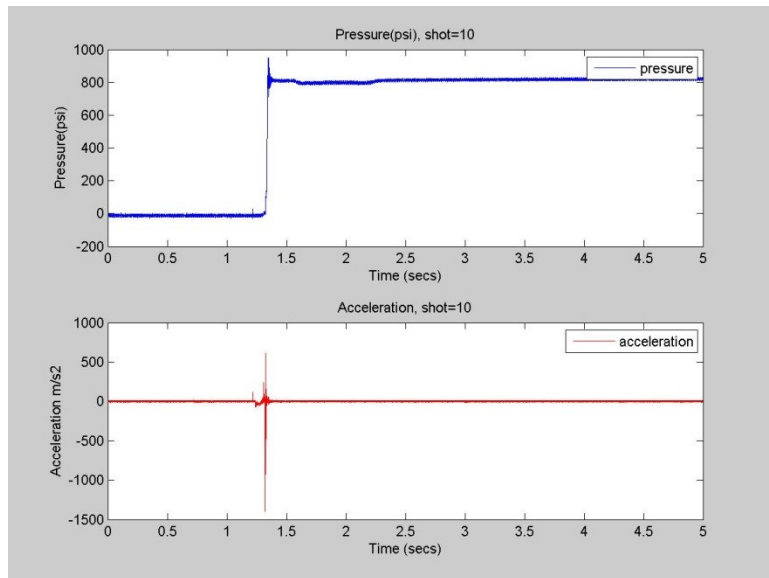


Figure A. 10 Pressure and Acceleration for Phase-2 Shot 10

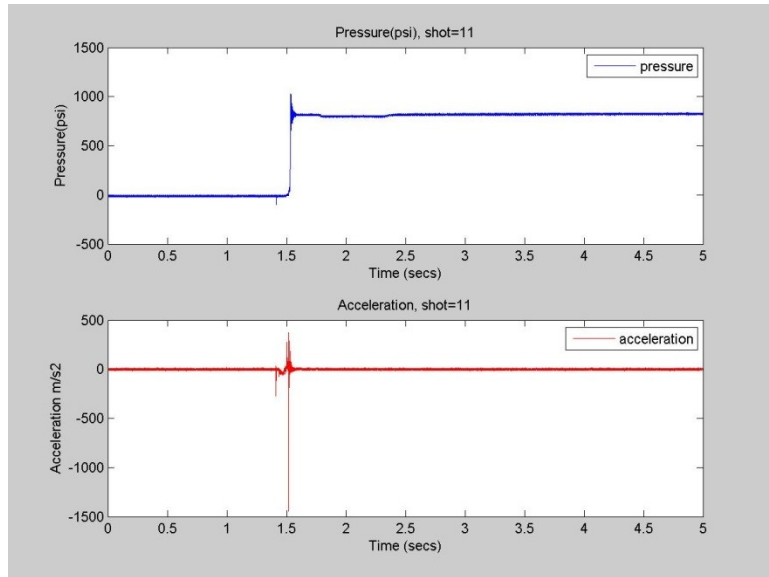


Figure A. 11 Pressure and Acceleration for Phase-2 Shot 11

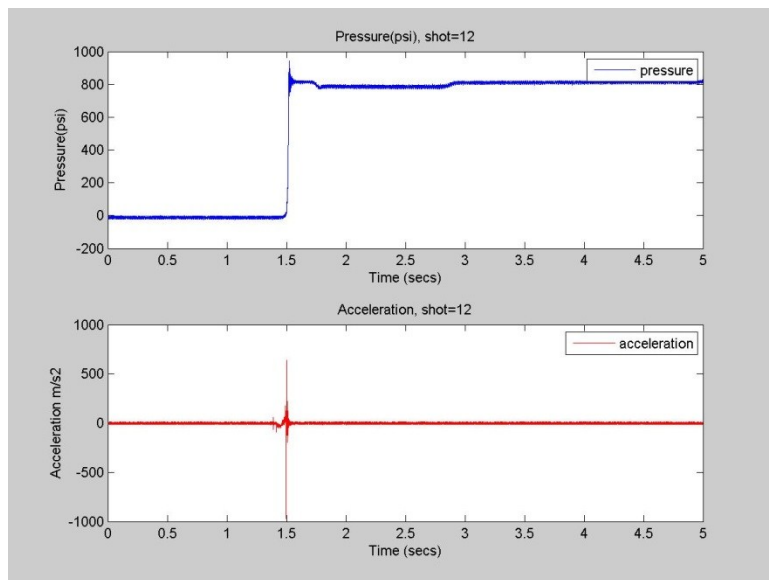


Figure A. 12 Pressure and Acceleration for Phase-2 Shot 12

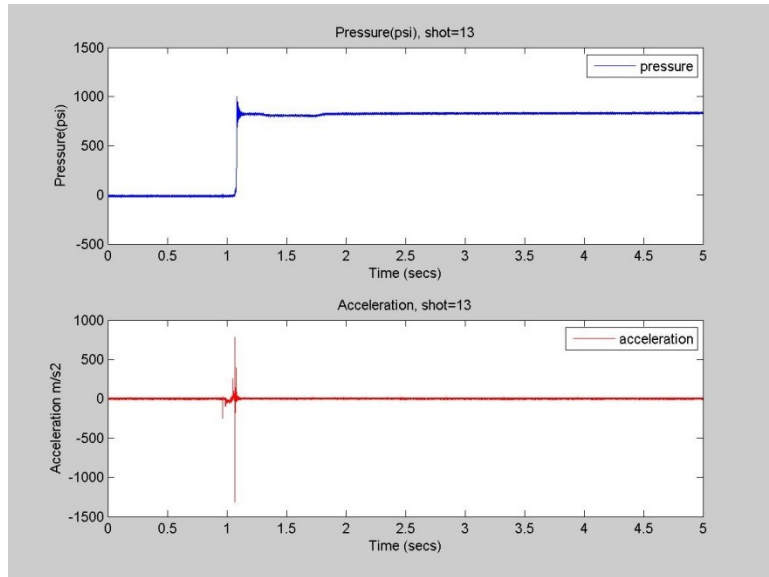


Figure A. 13 Pressure and Acceleration for Phase-2 Shot 13

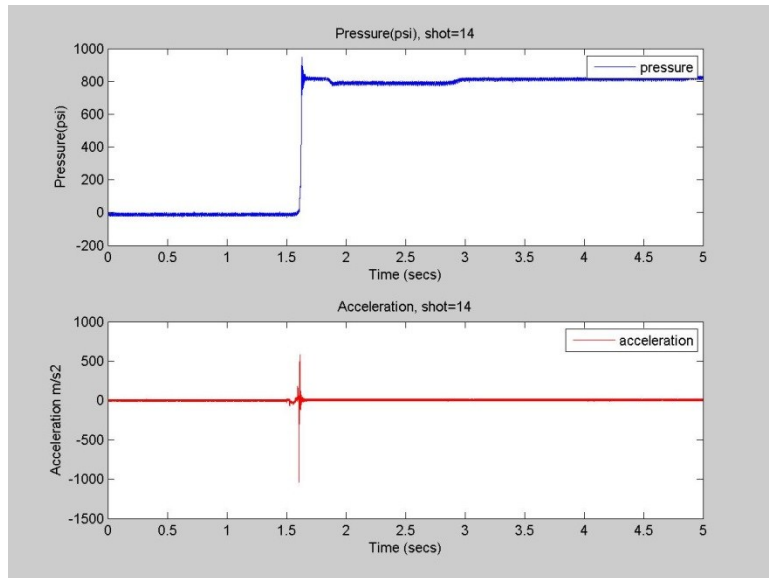


Figure A. 14 Pressure and Acceleration for Phase-2 Shot 14

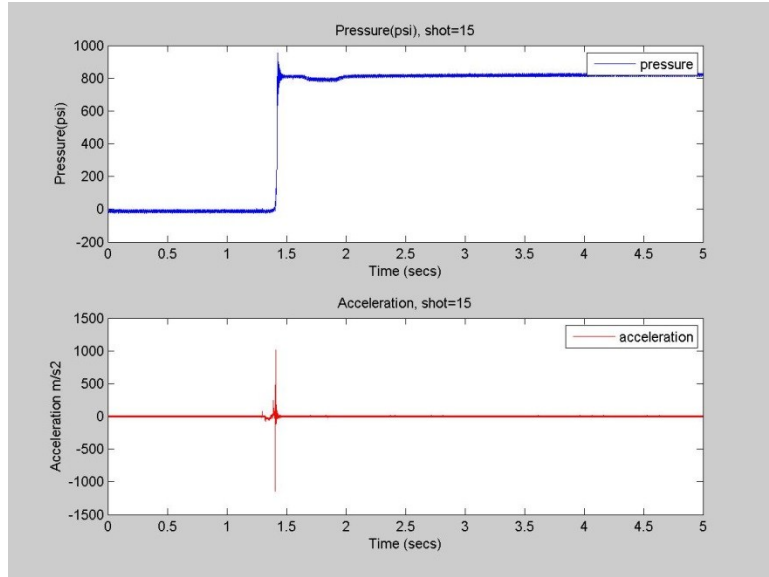


Figure A. 15 Pressure and Acceleration for Phase-2 Shot 15

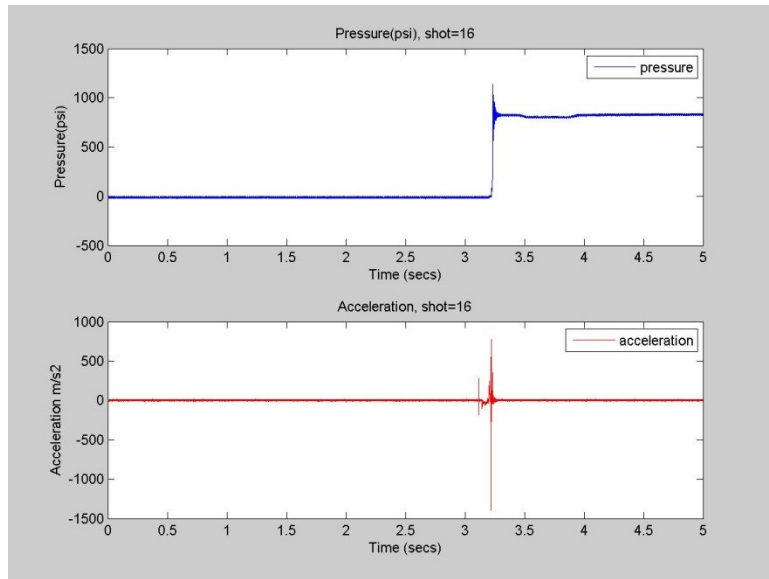


Figure A. 16 Pressure and Acceleration for Phase-2 Shot 16

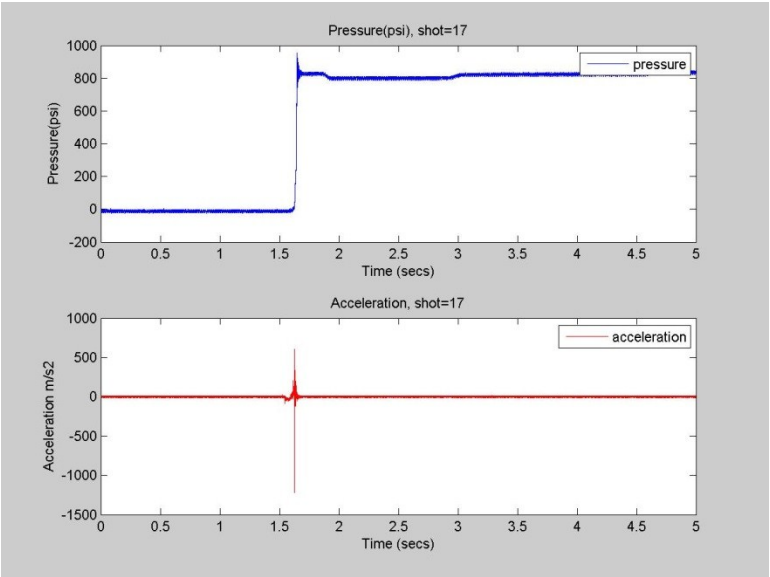


Figure A. 17 Pressure and Acceleration for Phase-2 Shot 17

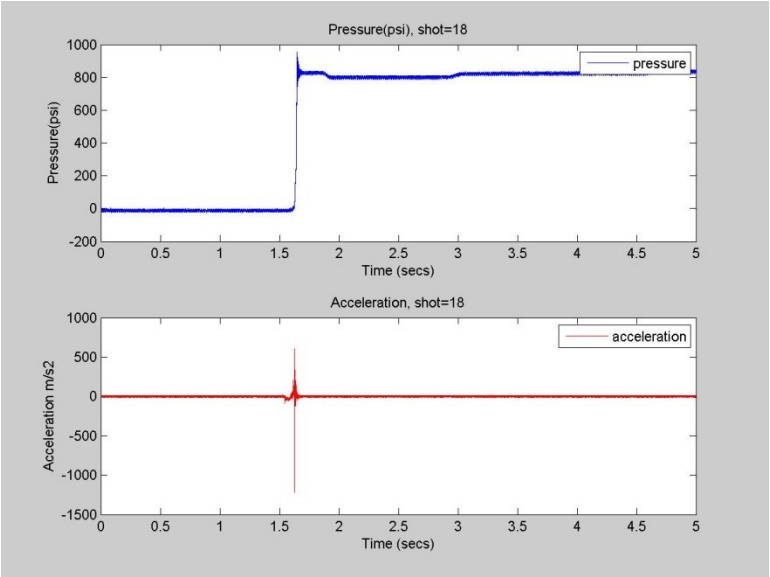


Figure A. 18 Pressure and Acceleration for Phase-2 Shot 18

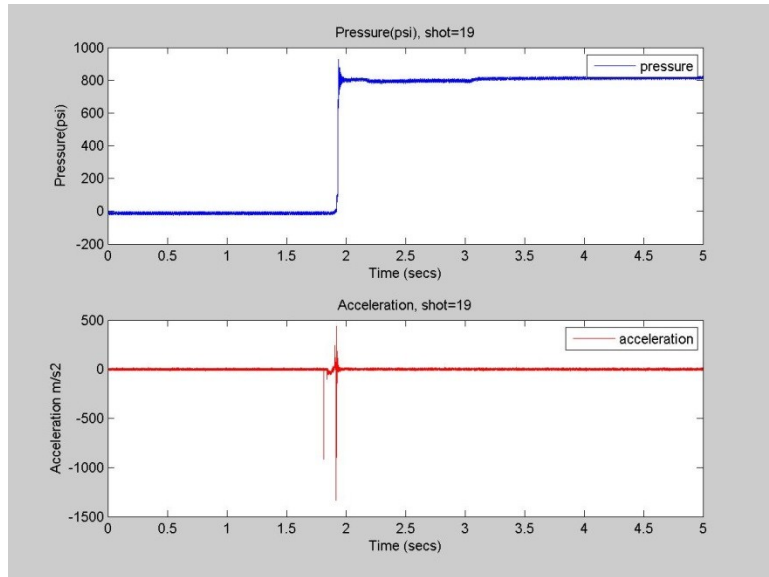


Figure A. 19 Pressure and Acceleration for Phase-2 Shot 19

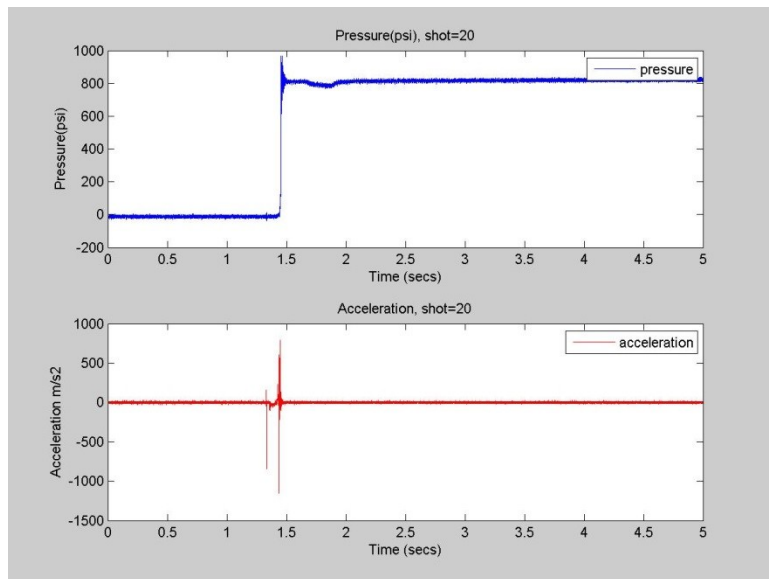


Figure A. 20 Pressure and Acceleration for Phase-2 Shot 20

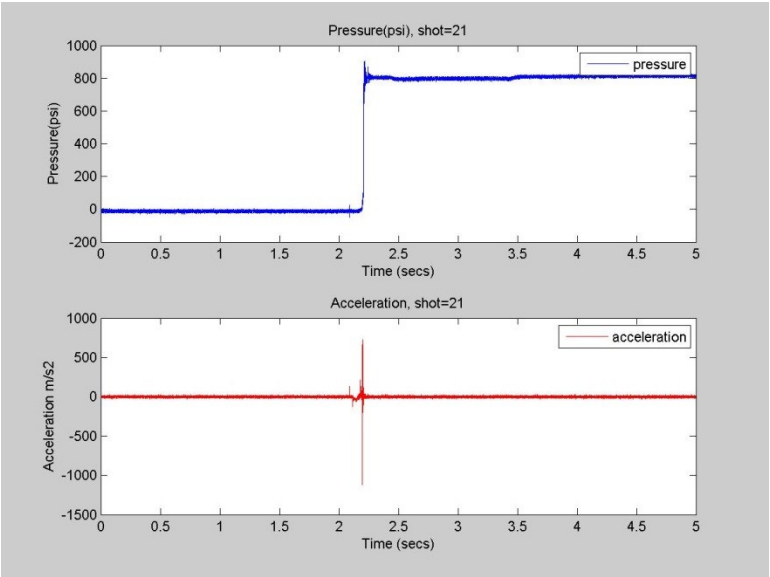


Figure A. 21 Pressure and Acceleration for Phase-2 Shot 21

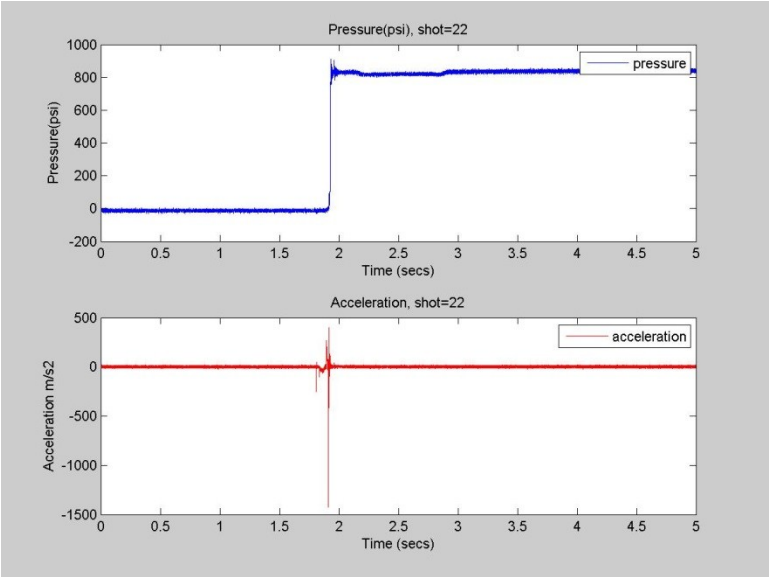


Figure A. 22 Pressure and Acceleration for Phase-2 Shot 22

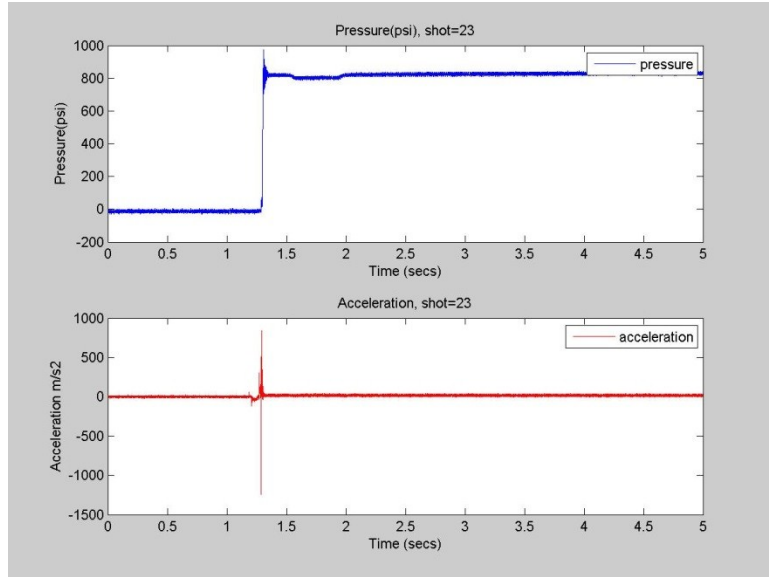


Figure A. 23 Pressure and Acceleration for Phase-2 Shot 23

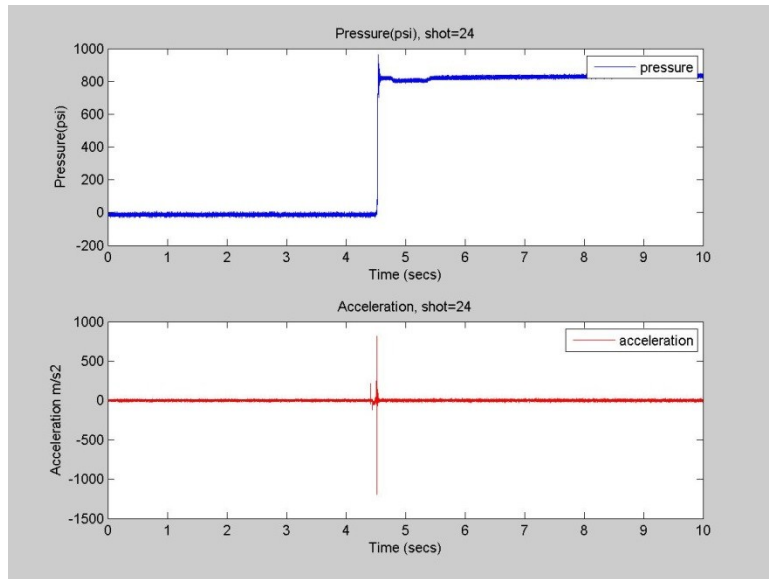


Figure A. 24 Pressure and Acceleration for Phase-2 Shot 24

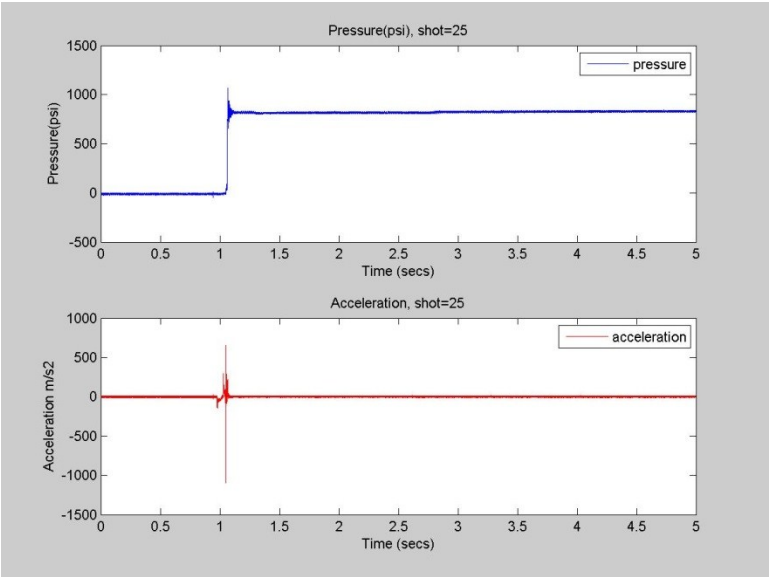


Figure A. 25 Pressure and Acceleration for Phase-2 Shot 25

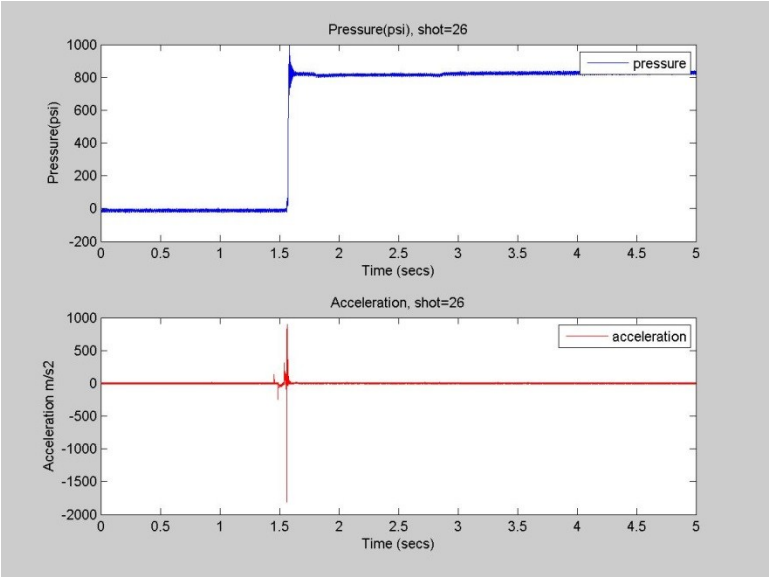


Figure A. 26 Pressure and Acceleration for Phase-2 Shot 26

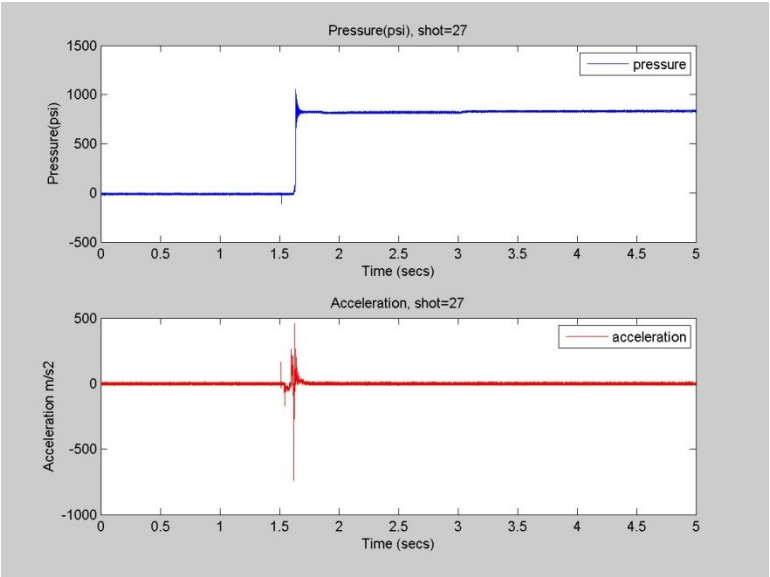


Figure A. 27 Pressure and Acceleration for Phase-2 Shot 27

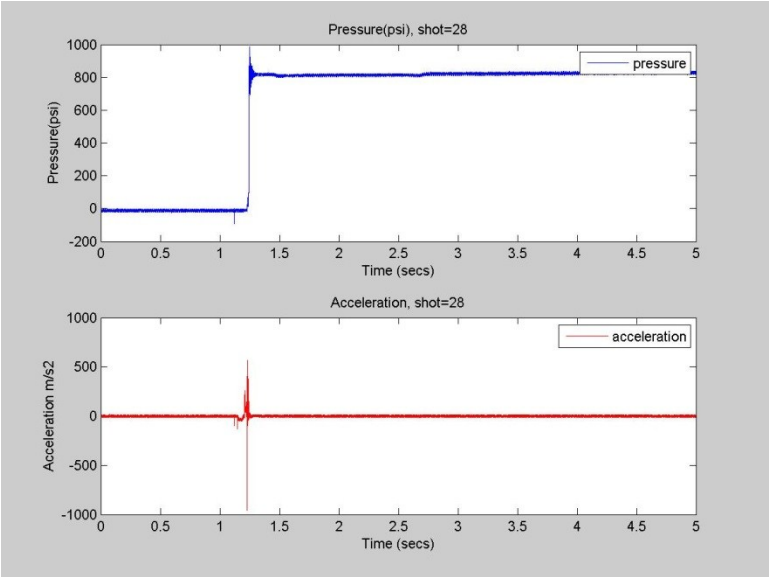


Figure A. 28 Pressure and Acceleration for Phase-2 Shot 28

APPENDIX B: SPECIFICATION SHEETS

TBR30 Bladder Accumulators

3,000 PSI (207 Bar)

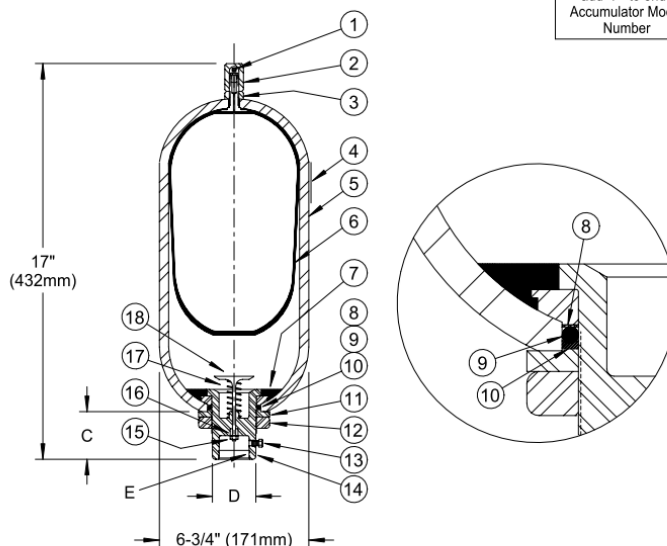


1 Gallon (4 Litres)

MODEL NUMBER	GAS CAPACITY		FLUID CAPACITY		DRY WEIGHT		DIMENSION				
	In. ³	Cm. ³	Gallons	Liters	Lbs.	Kg.	C		D		E
TBR30-1*	235	3,851	1	4	34	15	3-1/2	89	2-3/8	60	

* = BLADDER MATERIAL SUFFIX N = BUNA-N B = BUTYL H = EPR E = VITON

SAE -20 or 1-1/4" NPT available as standard. To specify 1-1/4" NPT - add "P" to end of Accumulator Model Number



GENERAL DESIGN DATA

MAXIMUM WORKING PRESSURE	3,000 PSI	(207 Bar)
MAXIMUM PROOF PRESSURE	4,500 PSI	(310 Bar)
MINIMUM BURST PRESSURE	12,000 PSI	(827 Bar)
OPERATING TEMPERATURE (Buna/Nitrile)	-20° TO +200° F	(-28° to 93° C)
BLADDER FOR PETROLEUM BASE OIL. SHELL ASME "U" STAMPED.		
INTERCHANGEABLE WITH MOST OTHER BRANDS.		

TBR30-1GAL ROP1 0908

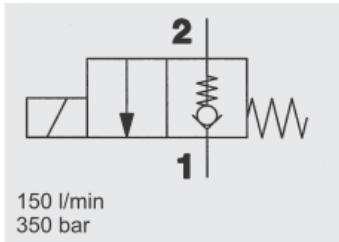
Phone: 803-245-5111 Fax: 803-245-2636 Tobul Accumulator, Inc. Bamberg, SC USA www.Tobul.com

Specification for Tobul accumulator

Table 1. NI USB-6008 and NI USB-6009 Comparison

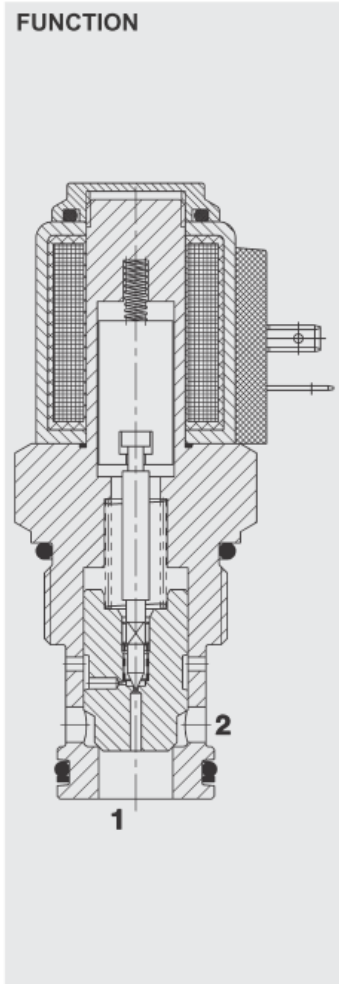
Feature	NI USB-6008	NI USB-6009
AI resolution	12 bits differential, 11 bits single-ended	14 bits differential, 13 bits single-ended
Maximum AI sample rate, single channel [*]	10 kS/s	48 kS/s
Maximum AI sample rate, multiple channels (aggregate) [*]	10 kS/s	48 kS/s
DIO configuration	Open collector [†]	Each channel individually programmable as open collector or active drive [†]
[*] System-dependent. [†] This document uses NI-DAQmx naming conventions. Open-drain is called open collector and push-pull is called active drive.		

Specification for NI 6009 USB DAQ Device



150 l/min
350 bar

FUNCTION



When the solenoid coil is not energized, the valve is closed from port 2 to port 1. Flow is permitted from port 1 to port 2.

When energized, there is free flow through the valve from port 2 to port 1. Return flow from port 1 to 2 is prevented.

E 5.945, 4/09, 13

2/2 Solenoid Directional Valve **UNF** Poppet Type, Pilot-Operated Normally Closed SAE-16 Cartridge – 350 bar WS16Z-01

FEATURES

- External surfaces zinc-plated and corrosion-proof
- Hardened and ground internal valve components to ensure minimal wear and extended service life
- Coil seals protect the solenoid system
- Wide variety of connectors available
- Excellent switching performance by high power HYDAC solenoid
- Low pressure drop due to CFD optimized flow path

SPECIFICATIONS

Operating pressure:	350 bar
Nominal flow:	max. 150 l/min up to 280 bar max. 100 l/min from 280 to 350 bar
Internal leakage:	Leakage-free (max. 5 drops = 0,25 cm ³ /min at 350 bar)
Media operating temperature range:	min. -20 °C to max. +100 °C
Ambient temperature range:	min. -20 °C to max. +60 °C
Operating fluid:	Hydraulic oil to DIN 51524 Part 1 and 2
Viscosity range:	7.4 to 420 mm ² /s
Filtration:	Class 21/19/16 according to ISO 4406 or cleaner
MTTF _a :	150 years (see "Conditions and instructions for valves" in brochure 5.300)
Installation:	No orientation restrictions
Material:	Valve body: steel Poppet: hardened and ground steel Seals: NBR (standard) FKM (optional, media temperature range -20 °C to 120 °C) Coil: Steel/Polyamide
Cavity:	FC16-2
Weight:	Valve complete: 0.62 kg Coil only: 0.19 kg

Electrical data

Response time:	Energized: approx. 50 ms De-energized: approx. 35 ms
Type of voltage:	DC solenoid, AC voltage is rectified using a bridge rectifier built into the coil
Current draw at 20 °C:	1.5 A at 12 V DC 0.8 A at 24 V DC
Voltage tolerance:	± 15 % of nominal voltage
Coil duty rating:	Continuous up to max. 115% of nominal voltage at max. 60° C ambient temperature
Coil type:	Coil...-40-1836

SPECIFICATIONS¹At T_A = -40°C to +105°C, 5.0 V dc ± 5%, acceleration = 0 g; unless otherwise noted.

Table 1.

Parameter	Conditions	Model No. AD22282			Model No. AD22283			Unit
		Min	Typ	Max	Min	Typ	Max	
SENSOR								
Output Full-Scale Range	I _{OUT} ≤ ±100 μA	120			250			g
Nonlinearity			0.2	2		0.2	2	%
Package Alignment Error				1			1	Degree
Cross-Axis Sensitivity			-5		+5	-5		+5
Resonant Frequency	V _{DD} = 5 V, 100 Hz		24			24		kHz
Sensitivity, Ratiometric (Over Temperature)			17.1	18	18.9	7.6	8	8.4
OFFSET								
Zero-g Output Voltage (Over Temperature) ²	V _{OUT} - V _{DD} /2, V _{DD} = 5 V	-125		+125	-100		+100	mV
NOISE								
Noise Density	10 Hz - 400 Hz, 5 V		3	10		5	15	mg/√Hz
Clock Noise				5			5	
FREQUENCY RESPONSE								
-3 dB Frequency	Two-pole Bessel	360	400	440	360	400	440	Hz
-3 dB Frequency Drift	25°C to T _{MIN} or T _{MAX}		2			2		Hz
SELF-TEST								
Output Change (Cube vs. V _{DD}) ³	V _{DD} = 5 V	400	500	600	200	250	300	mV
Logic Input High	V _{DD} = 5 V	3.5			3.5			V
Logic Input Low	V _{DD} = 5 V			1			1	V
Input Resistance	Pull-down resistor to GND	30	50		30	50		kΩ
OUTPUT AMPLIFIER								
Output Voltage Swing	I _{OUT} = ±400 μA	0.25		V _{DD} - 0.25	0.25		V _{DD} - 0.25	V
Capacitive Load Drive			1000			1000		
PREFILTER HEADROOM								
			800			1400		g
CFSR @ 400 kHz								
			2			1.5		V/V
POWER SUPPLY (V_{DD})								
Functional Range		4.75		5.25	4.75		5.25	V
Quiescent Supply Current	V _{DD} = 5 V	3.5		6	3.5		6	V
			1.5	2		1.5	2	mA
TEMPERATURE RANGE								
		-40		+125	-40		+125	°C

¹ All minimum and maximum specifications are guaranteed. Typical specifications are not guaranteed.² Zero g output is ratiometric.³ Self-test output at V_{DD} = (Self-Test Output at 5 V) × (V_{DD}/5 V)³.

GENERAL PURPOSE 5 OR 10 Vdc OUTPUT PRESSURE SENSORS

15 to 10,000 psi
1 to 690 bar



VOLTAGE OUTPUT
PRESSURE TRANSDUCERS
B

PX303/PX313 Series



- ✓ Welded Stainless Steel Construction
- ✓ NEMA 4 (IP65) Enclosure
- ✓ Reverse Polarity Protected
- ✓ Integral Strain Relief Cable or DIN Connector
- ✓ 0.25% Full Scale Accuracy

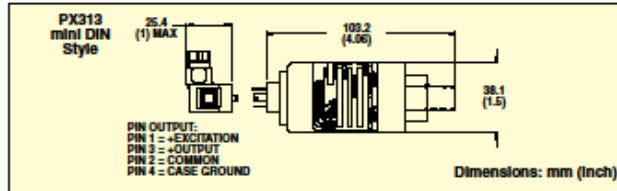
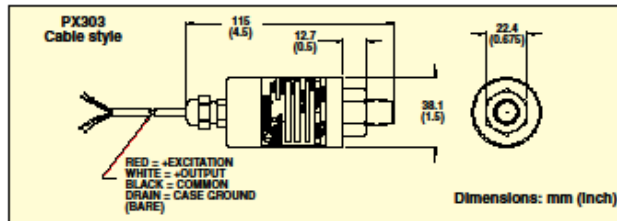
SPECIFICATIONS

5V Output (10V Output)
Excitation: 9 to 30 Vdc (14 to 30 Vdc) unregulated
Quiescent Current: 15 mA max
Output: 0.5 to 5.5 (1 to 11) Vdc
Accuracy: 0.25% FS (linearity, hysteresis, repeatability)
Zero Balance: ±2% FS
Span Tolerance: ±1% FS
Long-Term Stability: ±0.5% FS
Typical Life: 100 million cycles
Operating Temperature: -18 to 71°C (0 to 160°F)
Compensated Temperature: -1 to 71°C (30 to 160°F)
Total Thermal Effects: 1% FS max

PX303-2KG5V shown actual size.

Metric thread adaptors available, visit omega.com/mta_brk

PX313-100G5V shown actual size. DIN connector included.



Proof Pressure: 200%, 13,000 psi max
Min Load Resistance: 2000 Ω
Response Time: 1 ms
Cage Type: Stainless steel diaphragm, silicone oil-filled semiconductor sensor
Shock: 50 g @ 11 ms
Vibration: 15 g 10 to 2000 Hz
Wetted Parts: 17-4 PH and 300 Series stainless steel

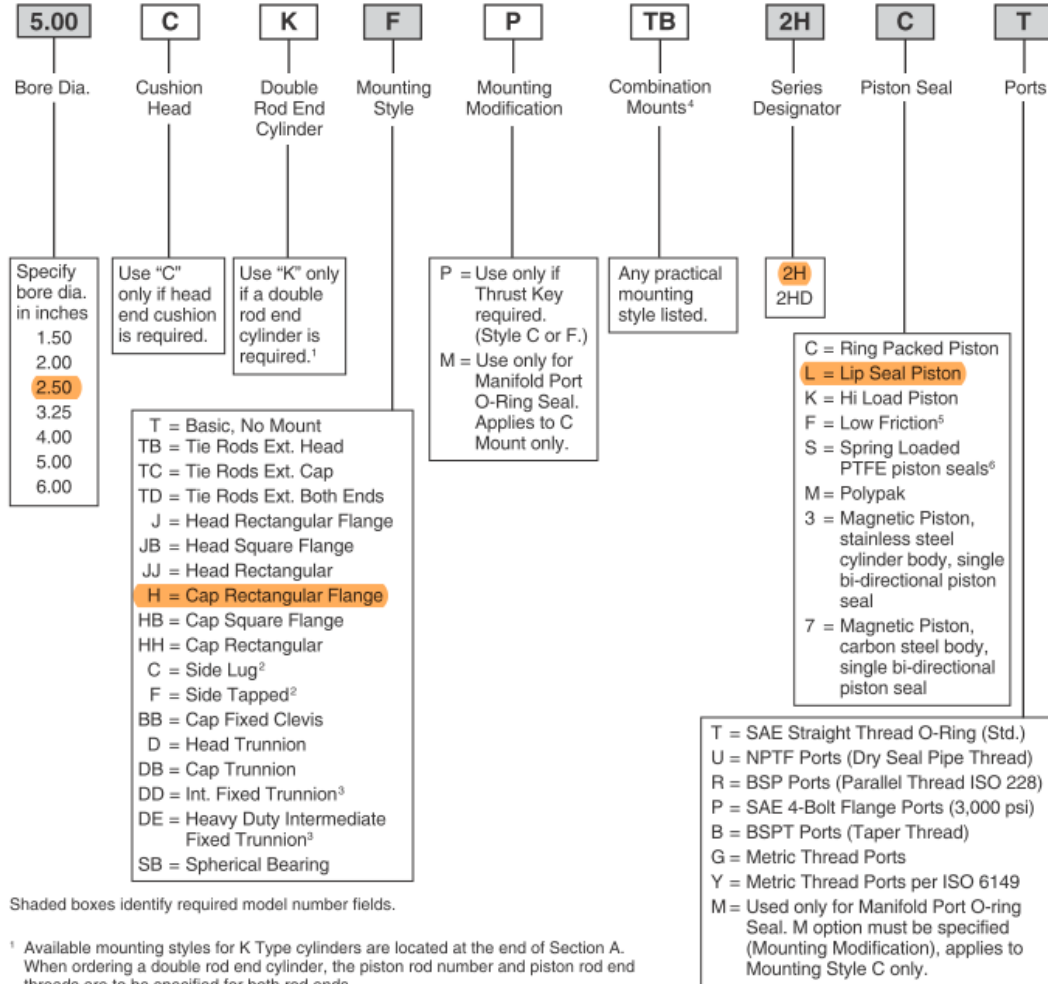
Pressure Port: 1/8 NPT male
Pressure Cavity: 0.075 in³
Electrical Connection:
PX303: 1 m (3') 4-conductor, 22 AWG, PVC jacketed, shielded cable
PX313: mini DIN connector (included)
Weight: 221 g (7.8 oz) to 1000 psi
 281 g (9.9 oz) from 1000 psi and higher

B-98

Specification for Omega pressure sensor

2H Model Code / How To Order

2H Model Code



Shaded boxes identify required model number fields.

¹ Available mounting styles for K Type cylinders are located at the end of Section A. When ordering a double rod end cylinder, the piston rod number and piston rod end threads are to be specified for both rod ends.

The model number should be created as viewing the primary rod end on the left hand side.

Example: K Type Cylinder:
4.00CKTD2HLT14A28AC10.000

² Mounting Styles C and F should have a minimum stroke length equal to or greater than their bore size.

³ Specify XI dimension.

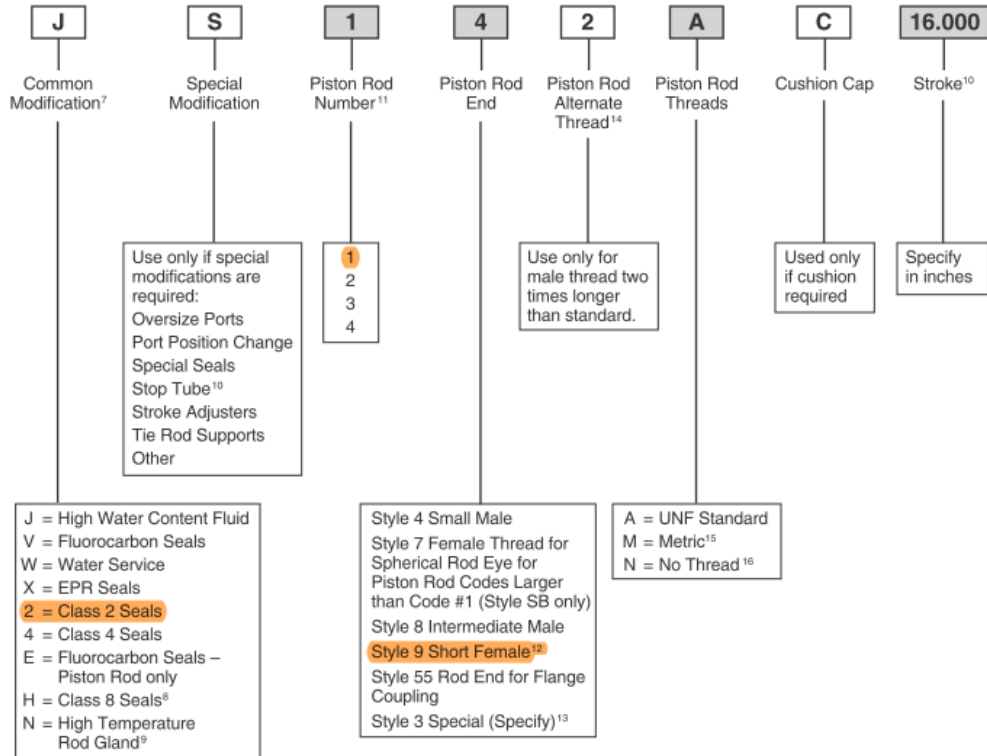
⁴ In general, the model numbers as read left to right corresponding to the cylinder as viewed from left to right with the primary end at the left. The second or subsequent mountings are mountings called out as they appear in the assembly moving away from the rod end. Except when tie rod extension mountings are part of a combination, all combinations should have a "S" (Special) in the model code and a note in the body of the order clarifying the mounting arrangement. The "P", as used to define a thrust key is not considered to be a mounting. However it is located at the primary end.

⁵ Low friction rod seals are also supplied when this option is selected.

⁶ Spring loaded PTFE piston seals are not available in 1.50, 2.00 and 2.50 bores with code 2 rod.



2H Model Code



Shaded boxes identify required model number fields.

Style 9 Minimum Stroke Table

Bore Ø	Rod Ø	Minimum Stroke
1.50 - 4.00	All	None
5.00	2.000	None
	2.500	1.000
	3.000	1.375
	3.500	1.625
6.00	2.500	None
	3.000	1.375
	3.500	1.375
	4.000	2.000

⁷ See common modifications Section D for additional options.
⁸ Class 8 piston seals will be cast iron rings (Piston Code C) in 1.50, 2.00 & 2.50 inch bores with code 2 rod. Spring loaded PTFE piston seals are not available in these bore and rod combinations. In all other bore and rod combinations, Piston Code S should be specified.
⁹ Energized PTFE rod seals & wiperseal. All other cylinder seals are fluorocarbon.
¹⁰ S = Stop Tube. Specify: stop tube length, net stroke and gross stroke.
 Gross stroke = stop tube length + net stroke. Gross stroke to be placed in the model number field.
 Example:
 2.000 inches long stop tube
 +14.000 inches net stroke
 16.000 inches gross stroke
¹¹ Refer to Rod buckling chart in Section E to assure rod number selected will not buckle under load.
¹² Style 9 stroke restrictions may apply. See Style 9 Minimum Stroke Table for details.
¹³ Provide dimensions for KK, A, W or WF. If otherwise special, furnish dimensioned sketch.
¹⁴ Available only in combination with Style 4 or Style 8.
¹⁵ See Section D for detailed information regarding standard metric rod end thread sizes.
¹⁶ Must be specified for Piston Rod End Style 55.



Specification for Parker hydraulic cylinder